bioRxiv preprint doi: https://doi.org/10.1101/2024.02.29.582524; this version posted March 2, 2024. The copyright holder for this preprint (which was not certified by peer review) is the author/funder, who has granted bioRxiv a license to display the preprint in perpetuity. It is made available under aCC-BY-NC-ND 4.0 International license.

The fungal protein Jps1 facilitates unconventional protein secretion through a direct phosphoinositide interaction

Sanchi Dali[1], Michèle Schultz[1], Marian Köster[1], Michael Kamel[2], Max Busch[2], Wieland Steinchen[3,4], Sebastian Hänsch[5], Jens Reiners[6], Sander Smits[6], Alexej Kedrov[2], Florian Altegoer[1#], Kerstin Schipper[1#]

[1] Institute of Microbiology, Heinrich Heine University Düsseldorf, Universitaetsstr. 1, 40225 Düsseldorf, Germany

[2] Synthetic Membrane Systems, Institute for Biochemistry, Heinrich Heine University Düsseldorf, Universitaetsstr. 1, 40225, Düsseldorf, Germany

[3] Department of Chemistry, Philipps University Marburg, Hans-Meerwein-Straße 4, 35043 Marburg, Germany

[4] Center for Synthetic Microbiology, Philipps University Marburg, Karl-von-Frisch-Straße 14, 35043 Marburg, Germany

[5] Center of Advanced Imaging (CAi), Heinrich Heine University Düsseldorf, Universitaetsstr. 1, 40225, Düsseldorf, Germany

[6] Center for Structural Studies, Heinrich Heine University Düsseldorf, Universitaetsstr. 1, 40225, Düsseldorf, Germany

[#]Shared correspondence: kerstin.schipper@hhu.de; florian.altegoer@hhu.de

Running title

Insights into the lipid interaction mechanism of Jps1

Keywords

cytokinesis, unconventional secretion, protein-lipid interaction, fungi, liposome, membrane binding

bioRxiv preprint doi: https://doi.org/10.1101/2024.02.29.582524; this version posted March 2, 2024. The copyright holder for this preprint (which was not certified by peer review) is the author/funder, who has granted bioRxiv a license to display the preprint in perpetuity. It is made available under aCC-BY-NC-ND 4.0 International license.

Abstract

Protein secretion is indispensable for essential cellular processes in eukaryotic cells, contributing significantly to nutrient acquisition, defense or communication. Alternative pathways bypassing the endomembrane system collectively referred to as unconventional secretion are gaining increasing attention. A number of important molecules such as cytokines, fibroblast growth factor or viral proteins are being exported through these mechanistically diverse pathways. In the fungal model *Ustilago maydis*, cytokinesis-dependent unconventional secretion mediates export of the chitinase Cts1 via the fragmentation zone. This membrane-rich compartment is formed during cytokinesis between mother and daughter cells. Recently, we identified Jps1, a previously uncharacterized protein, as a crucial factor for Cts1 localization and export. Combining biochemical experiments and *in vivo* studies, we here uncover two pivotal features of Jps1: phosphoinositide (PIP) binding and dimerization. Our findings reveal that Jps1 does not harbor a canonical PIP-binding domain but instead specifically binds to $PI(4,5)P_2$, likely via basic residues. A conserved structural core domain of Jps1 mediates dimerization, while the flexible variable regions suggest potential diversification in different basidiomycetous species. The accumulation of Jps1 in the fragmentation zone, facilitated by its PIP affinity, provides a direct membrane recognition mechanism. This discovery sheds light on a previously unknown key feature of Jps1, elucidating its role in supporting Cts1 secretion, and representing a crucial step towards understanding the broader implications of unconventional secretion in eukaryotic cells.

bioRxiv preprint doi: https://doi.org/10.1101/2024.02.29.582524; this version posted March 2, 2024. The copyright holder for this preprint (which was not certified by peer review) is the author/funder, who has granted bioRxiv a license to display the preprint in perpetuity. It is made available under aCC-BY-NC-ND 4.0 International license.

Introduction

Eukaryotic cells rely on an intricate network of protein secretion pathways to fulfill vital functions essential for survival. These pathways are crucial for tasks like acquiring nutrients, building defenses, and communicating with other cells. In eukaryotic cells, secretion was long thought to predominantly occur via the endomembrane system (Schekman 2010). Here, proteins destined for secretion are targeted to the Endoplasmic reticulum (ER) via N-terminal signal peptides (Walter and Blobel 1980, Lee, Miller et al. 2004, Rapoport 2007). After entry of the ER through the Sec61 translocon, the proteins undergo folding and are eventually modified, for example by *N*-glycosylation and disulfide bonds (Viotti 2016). Besides this well-established secretion via the endomembrane system, various unconventional secretion routes where proteins are exported despite the lack of N-terminal signal sequences were unveiled in recent years (Rabouille 2017, Dimou and Nickel 2018, Nickel and Rabouille 2018). Unconventional secretion of soluble proteins can be grouped into mechanisms of direct translocation through the plasma membrane via direct translocation (type I) or ABC transporters (type II) and export pathways that employ vesicular intermediates (type III) (Rabouille, Malhotra et al. 2012). A prominent example for direct translocation is the secretion of mammalian Fibroblast Growth Factor 2 (FGF2), a proangiogenic mitogen, from tumor cells (Sparn, Meyer et al. 2022). This protein is recruited to the plasma membrane via interaction with phosphatidyl inositol 4,5 phosphate (PI4,5P) (Steringer and Nickel 2018, Joliot 2023). At the membrane it assembles into lipidic toroidal pores that surpass the membrane and mediate export of FGF2 monomers (Brough, Pelegrin et al. 2017). Translocation critically depends on phosphorylation via TEC kinase at the membrane. In addition, extracellular heparan sulfates play a crucial role in supporting export by binding FGF2 with high affinity (Zehe, Engling et al. 2006, Steringer and Nickel 2018). Interestingly, unconventional secretion mechanisms of other important proteins like HIV-Tat or interleukin 1-β share at least some of the features that have been described for FGF2 export (Dimou and Nickel 2018).

Unconventional secretion has not only been observed in mammalian cells but is also conserved in lower eukaryotes such as fungi. Here, important examples are superoxide dismutase and acyl-CoA binding protein which are secreted by a type III mechanism and have been intensively studied in *Saccharomyces cerevisiae* (Cruz-Garcia, Malhotra et al. 2018). Both proteins are exported by nutrient-starvation induced unconventional secretion that relies on the Golgi reassembling and stacking protein (GRASP) homolog Grh1 and multiple components of the endosomal sorting complexes required for transport (ESCRT) (Duran, Anjard et al. 2010). More specifically, a diacidic motif is exposed upon starvation(Cruz-Garcia, Brouwers et al. 2017), determining capture of the cargo into Grh1 containing so-called compartments of unconventional secretion (CUPS), that are derived from the Golgi apparatus

bioRxiv preprint doi: https://doi.org/10.1101/2024.02.29.582524; this version posted March 2, 2024. The copyright holder for this preprint (which was not certified by peer review) is the author/funder, who has granted bioRxiv a license to display the preprint in perpetuity. It is made available under aCC-BY-NC-ND 4.0 International license.

and from endosomes. The CUPS likely serve as sorting stations for export (Cruz-Garcia, Malhotra et al. 2018). Unconventional secretion mechanisms of many other proteins are often not fully understood. Nevertheless, this evolving landscape of alternative export pathways highlight the complexity and versatility of cellular mechanisms, expanding our understanding from canonical to unconventional secretion processes.

In *Ustilago maydis*, a cytokinesis-dependent unconventional secretion mechanism was demonstrated crucial for export of the chitinase Cts1 (Stock, Sarkari et al. 2012, Reindl, Hansch et al. 2019). In cylindric yeast cells of this fungal model, cytokinesis is initiated by the formation of a small bud at one of the cell poles which extends by polar growth. After nuclear division, physical separation is initiated by the formation of a primary septum at the mother cell side. The septum acts as a physical barrier and separates the cytoplasm of the two cells. Consecutively, a secondary septum is formed at the daughter cell side, delimiting a membrane-rich so-called fragmentation zone (Altamirano, Chandrasekaran et al. 2017). Strains lacking chitinases Cts1 and Cts2 are not able to separate and form tree-like structures, indicating that both enzymes contribute to physical cell separation (Langner and Gohre 2016). Interestingly, while Cts2 contains a classical signal peptide this is lacking in Cts1 while it is still active extracellularly (Stock, Sarkari et al. 2012). We have demonstrated that this enzyme is exported by an unconventional mechanism, that involves Cts1 recruitment from the daughter cell to the primary septum. The enzyme then localizes to the fragmentation zone where it participates in cell separation presumably by hydrolyzing remnant chitin (Stock, Sarkari et al. 2012, Langner and Gohre 2016, Reindl, Stock et al. 2020).

Recently, we used a forward genetic screen to identify factors involved in unconventional secretion of Cts1 and discovered the yet uncharacterized protein Jps1 (Reindl, Stock et al. 2020). *jps1* deletion mutants show mis-localized Cts1 that is excluded from the fragmentation zone and a strongly diminished extracellular chitinase activity, supporting its essential role for Cts1 export (Reindl, Stock et al. 2020). Jps1 lacks a predicted signal peptide but is present in the culture supernatant, indicating that it is also exported unconventionally (Philipp, Hussnaetter et al. 2021). In line with that, Jps1 is enriched in the fragmentation zone, as observed for Cts1, and yeast-two hybrid data support the idea of a direct interaction (Reindl, Stock et al. 2020). Hence, we hypothesized that Jps1 might be an anchoring factor that recruits or tethers Cts1 to the fragmentation zone. Here, we now present an in-depth biochemical analysis of Jps1, revealing an unusual mode of $PI(4,5)P_2$ binding and the presence of a core domain that mediates dimerization. Interestingly, these features are conserved across different orthologs in the basidiomycete phylum. Our findings are in line with the essential function of Jps1 in the membrane-rich fragmentation zone and provide new insights into this mechanism of unconventional secretion.

bioRxiv preprint doi: https://doi.org/10.1101/2024.02.29.582524; this version posted March 2, 2024. The copyright holder for this preprint (which was not certified by peer review) is the author/funder, who has granted bioRxiv a license to display the preprint in perpetuity. It is made available under aCC-BY-NC-ND 4.0 International license.

Results

Jps1 is a conserved basidiomycete-specific protein with a central core domain

Our previous work identified Jps1 as an essential factor for unconventional secretion in *U. maydis* (Reindl, Stock et al. 2020). No information on the function of Jps1 was available from public databases and domain prediction tools did not reveal any known functional domains. We therefore performed a phylogenetic search using BlastP (https://blast.ncbi.nlm.nih.gov/Blast.cgi) with the 609 amino acids sequence of *U. maydis* Jps1 protein as a query to identify conserved patches that might hint to functionally relevant regions. We identified orthologs widespread but restricted to basidiomycetes. In total, more than 1,000 homologs of Jps1 were identified across these different basidiomycete species. We observed a large variability in sequence length, ranging from ~185 to more than 1,000 amino acids. Consistently, a region covering residues 356-480 of the *U. maydis* Jps1 variant, showed an overall high conservation (35-53 % sequence identity) across all species, while the N- and C-terminal regions had a high degree of variability in the amino acid sequence and length (**Fig. S1**). Notably, this conserved region is also present in short Jps1 versions, as e.g. the one of *Hebeloma cylindrosporum* that only consists of 287 amino acids (**Fig. S1**).

To gain a better understanding of the architecture of Jps1, we used AlphaFold2 to predict a structural model of the protein (**Fig. S2**). As we did not have prior information of the oligomeric state of Jps1, we also predicted homodimers, trimers and tetramers using AlphaFold2-Multimer (Jumper, Evans et al. 2021). The Jps1 monomer showed two regions with intermediate pLDDT values (>80), while the aforementioned conserved region had high pLDDT values of >90 (**Fig. S2A**). Predicting a Jps1 dimer elevated the pLDDT in the conserved regions from around 70-80 to >95, while it strongly dropped in the less conserved regions supporting the presence of intrinsically disordered regions (**Fig. S2A, B**). Prediction of higher oligomers did not improve the pLDDT as observed for the dimer (data not shown). Our structural model suggests that Jps1 has unstructured N- and C-termini and a central domain that is assembled from several structured parts within the N-terminus and the conserved core domain (**Fig. 1A, B**). This core domain consists of 8 β-strands and a total of 11 α-helices (**Fig. 1B**). Six of the β-strands (β1, 2, 5-8) form a central β-sheet that is framed by helices α1-4, 7 and helices α10-12 on the other side (**Fig. 1B**). Helices α8, 9 and the two β-strands 3 and 4 form a small domain that is stacked onto the central β-sheet (**Fig. 1B**). This central domain is apparently not only formed by the above-mentioned core region of Jps1 but residues located N-terminally also contribute (e.g. α1-α7 and β1, β2 and β3). Three flexible loop regions (LR) surround the compact protein core (LR1-LR3, **Fig. 1A, B**).

bioRxiv preprint doi: https://doi.org/10.1101/2024.02.29.582524; this version posted March 2, 2024. The copyright holder for this preprint (which was not certified by peer review) is the author/funder, who has granted bioRxiv a license to display the preprint in perpetuity. It is made available under aCC-BY-NC-ND 4.0 International license.

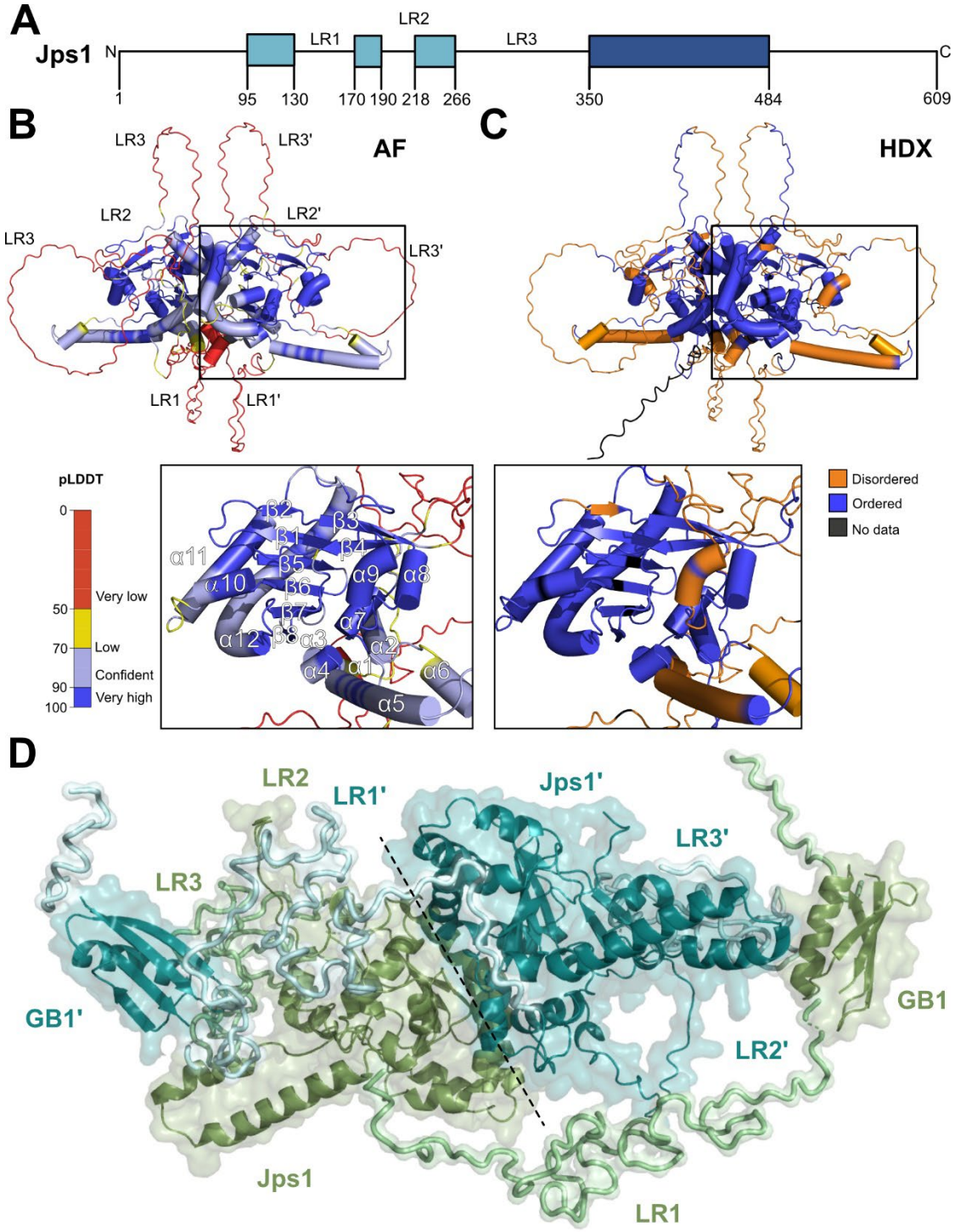

Figure 1: Structure prediction and HDX-MS reveal a flexible architecture of Jps1. A. Domain architecture of Jps1 based on the structural prediction (AF) and HDX-MS analysis. Boxes indicate structured patches, while the coloring reflects less conserved regions (light blue) and the region strongly conserved across basidiomycetes (dark blue). LR: Loop regions. **B.** Structural model of the Jps1 dimer predicted with AlphaFold2 (AF) (Jumper, Evans et al. 2021) shown in cartoon representation and colored according to the model confidence. **C.** Structural model of the Jps1 dimer colored according to HDX-MS exchange. Disordered and ordered regions and those not covered in HDX-MS (HDX) are colored in red, blue and black in the AlphaFold2 model of Jps1, respectively. Below the two panels, a close-up of the central core domain is shown. Secondary structure elements are labeled accordingly. **D.** Rigid-body modeling of the Jps1 dimer based on small-angle X-ray scattering data. The two protomers, Jps1 and Jps1', are colored in smudge green and cyan, respectively.

bioRxiv preprint doi: https://doi.org/10.1101/2024.02.29.582524; this version posted March 2, 2024. The copyright holder for this preprint (which was not certified by peer review) is the author/funder, who has granted bioRxiv a license to display the preprint in perpetuity. It is made available under aCC-BY-NC-ND 4.0 International license.

To support our bioinformatic analysis on Jps1 and gain information on its biochemical properties, we heterologously produced Jps1 as GB1 fusion in *Escherichia coli* and purified the soluble protein through a two-step purification procedure consisting of Ni-NTA affinity chromatography followed by size-exclusion chromatography (**Fig. S3A**). We subjected the purified Jps1 to hydrogen-deuterium exchange mass spectrometry (HDX-MS) to validate the structured and flexible regions of Jps1 suggested by our structural model. Mapping our HDX-MS results revealed that most of the Jps1 residues inferred as disordered in the AlphaFold2 model reach their maximal deuterium incorporation already after ten seconds of HDX while those constituting the core domain exhibit protection against fast HDX indicative for the presence of secondary or higher-order structures (**Figs. 1C, S4**). This suggests that Jps1 adopts a conformation that is reminiscent of its structural model in solution. To further confirm these findings, we also performed small-angle X-ray scattering (SAXS) experiments. Here, we generated a Jps1 version lacking the unstructured C-terminal residues (Jps1$^{1-484}$) as this region does not contribute to the structured core domain and a large number of disordered residues complicates the *ab initio* modeling. Our SAXS experiments confirmed an overall compact architecture of the Jps1 dimer with some elongated regions as judged from the intra-particle distance and the Kratky plot (**Fig S5, Table S1**). We also performed rigid body modeling of Jps1, which suggested that the loop regions (**Fig. 1B**) most likely align more closely to the protein core (**Fig. 1D**). In conclusion, a combination of bioinformatic and biochemical experiments revealed that Jps1 is a basidiomycete-specific protein with a core domain enclosed by flexible regions.

Jps1 dimerizes via the C-terminal core domain

To further characterize Jps1 and confirm the predicted dimer, we performed size-exclusion chromatography coupled multi-angle light scattering (SEC-MALS). Jps1 eluted in one stable fraction from the SEC, while MALS revealed the presence of a single species of 134 ± 3.5 kDa indicating the formation of homodimers based on the calculated MW of 63 kDa of a Jps1 monomer (**Fig. 2A**). In addition, we also performed mass photometry experiments using a nanomolar concentration (10 nM) of Jps1 showing that 69% of all particles were in a single fraction at 125 kDa matching the molecular weight of dimers, with only a small subfraction of 9% at 64 kDa (**Fig. 2B**). Small angle X-ray scattering (SAXS) experiments also revealed a predominantly dimeric species in solution (**Tab. S1**).

To identify the region of Jps1 that mediates the homodimerization, we tested the previously mentioned truncated version lacking the unstructured C-terminus (Jps1$^{1-484}$) and an N-terminal version lacking the conserved domain (Jps1$^{1-218}$), again fused to an N-terminal GB1-tag (**Fig. 2C**). Both truncated Jps1 constructs could be expressed and purified to homogeneity using the same purification procedure as described for the full-length Jps1 version including the GB1-tag (**Fig. S6A**) and employed for mass photometry measurements.

bioRxiv preprint doi: https://doi.org/10.1101/2024.02.29.582524; this version posted March 2, 2024. The copyright holder for this preprint (which was not certified by peer review) is the author/funder, who has granted bioRxiv a license to display the preprint in perpetuity. It is made available under aCC-BY-NC-ND 4.0 International license.

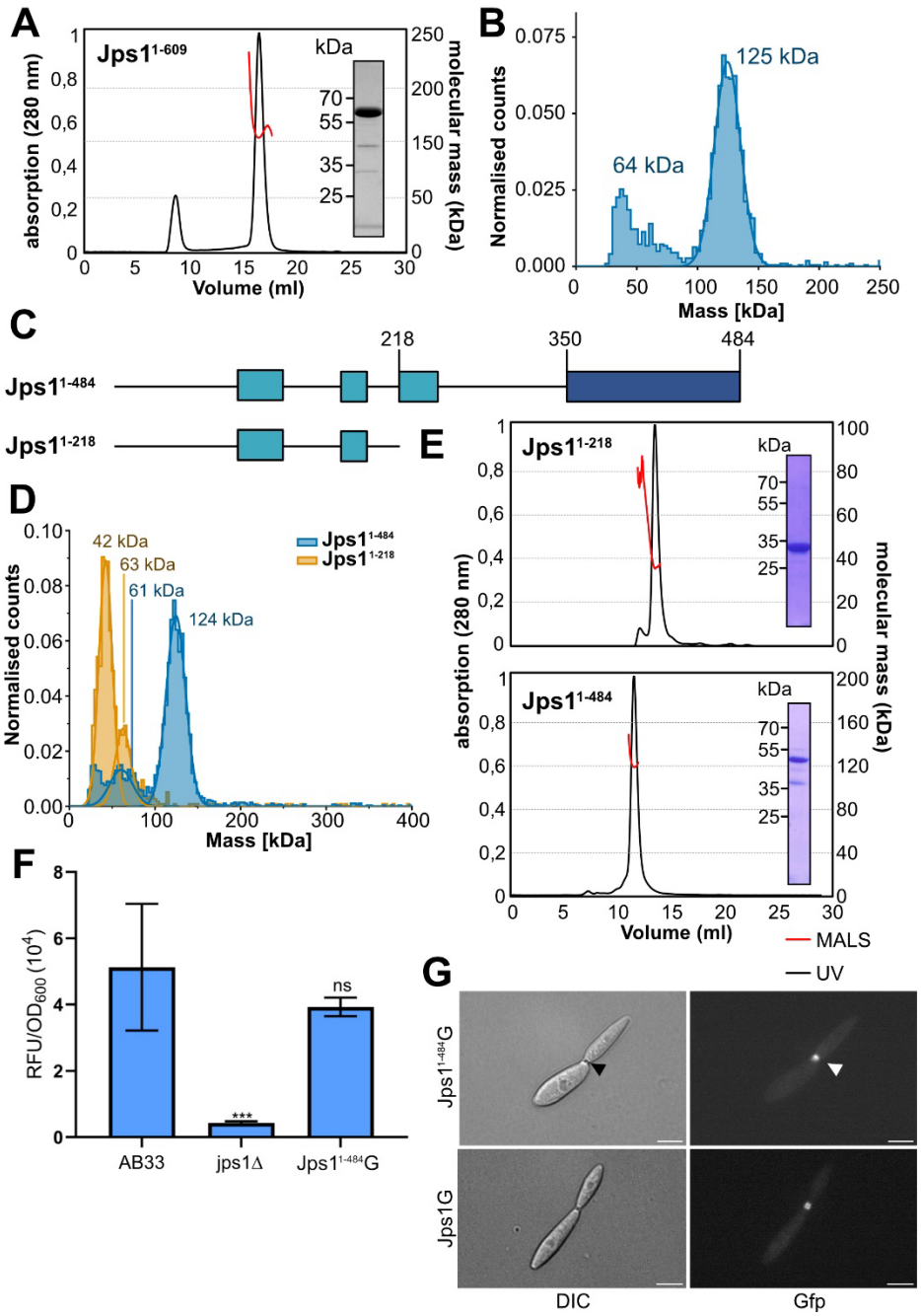

Figure 2: Biochemical analysis of *U. maydis* Jps1 supports homodimer formation. A. Multi-angle-light scattering coupled SEC (SEC-MALS) of full length recombinant UmJps1 (Jps1$^{1-609}$). The black line shows the absorption at 280 nm (SEC), the molecular weight as determined by MALS is depicted in red. Inset: SDS-PAGE of purified protein before SEC-MALS **B.** Mass photometry of recombinant UmJps1 at a concentration of 10 nM. **C.** Schematic representation of the protein architecture of the two truncated UmJps1 versions Jps1$^{1-484}$ and Jps1$^{1-218}$ Boxes indicate structured patches, while the coloring reflects less conserved regions (light blue) and the region strongly conserved across basidiomycetes (dark blue). **D.** Mass photometry of the two variants UmJps1$^{1-484}$ and UmJps1$^{1-218}$ at a concentration of 10 nM. **E.** SEC-MALS of UmJps1$^{1-484}$ and UmJps1$^{1-218}$. The black line shows the absorption at 280 nm (SEC), the molecular weight as determined by MALS is depicted in red. Insets: SDS-PAGE of purified proteins before SEC-MALS. **F.** Extracellular Cts1 activity of indicated AB33 derivatives. Error bars depict standard deviation. ***P-value 0.001; n.s., not significant (two sample t-test). **G.** Fluorescence microscopic localization of Jps1G and the truncated version Jps1$^{1-484}$G in yeast-like growing cells AB33 jps1Δ derivatives. DIC, Differential interference contrast. Scale bars, 10 µm.

bioRxiv preprint doi: https://doi.org/10.1101/2024.02.29.582524; this version posted March 2, 2024. The copyright holder for this preprint (which was not certified by peer review) is the author/funder, who has granted bioRxiv a license to display the preprint in perpetuity. It is made available under aCC-BY-NC-ND 4.0 International license.

Experiments on GB1-Jps1$^{1-218}$ revealed a dominant fraction at 42 kDa and a small subfraction at 63 kDa, while for GB1-Jps1$^{1-484}$ similar results as for the full-length Jps1 were observed (**Fig. 2D**). MALS of the purified variants also indicated a molecular weight of 36.5 ± 1.9 kDa of GB1-Jps1$^{1-218}$ suggesting a monomer while GB1-Jps1$^{1-484}$ formed dimers comparable to the full-length protein with a molecular mass of 117.2 ± 1.1 kDa (**Fig. 2E**).

Earlier results from the forward genetic screen demonstrate that three Jps1 versions that are truncated by insertion of a premature stop codon within the conserved core domain are not functional (Reindl, Stock et al. 2020). To assess whether the protein version with the complete core domain but lacking the adjacent flexible C-terminal region is still functional, we expressed a construct for Jps1$^{1-484}$ fused to Gfp (Jps1$^{1-484}$G) in a *jps1* deletion strain (AB33 jps1Δ/Jps1$^{1-484}$G). *In vivo* studies revealed full complementation of extracellular Cts1 activity, suggesting that the truncated protein is fully functional in mediating unconventional Cts1 secretion (**Fig. 2F**). In accordance, fluorescence microscopic inspection of the respective strains confirmed the localization of Jps1$^{1-484}$G in the fragmentation zone of dividing cells (**Fig. 2G**). In essence, the conserved C-terminal domain of Jps1 mediates homodimerization while the adjacent flexible C-terminal region is dispensable for the protein function.

Jps1 orthologs homodimerize but exhibit functional diversification

Our phylogenetic analysis suggested that the core domain is conserved across fungal species, while the surrounding regions show a high sequence variability (**Fig. S1**). We were therefore interested whether dimerization is a conserved feature of Jps1 and whether orthologs can functionally complement the *jps1* deletion. Two Jps1 orthologs were selected for recombinant production in *E. coli*: A long version from the very close relative *Sporisorium reilianum* (Sorghum smut, SrJps1; calculated molecular weight of 77 kDa) and a short Jps1 version from the mushroom *Hebeloma cylindrosporum* (HcJps1; 38 kDa). Both versions were well-expressed as soluble GB1-fusions and could be purified as described previously (**Fig. S6B**). SEC-MALS revealed that SrJps1 and HcJps1 constituted dimers with apparent molecular masses of 153.2 ± 2.7 kDa and 77.8 ± 0.6 kDa, respectively (**Fig. 3A**). Notably, mass photometry suggested that SrJps1 formed predominantly dimers, while we observed mostly monomeric species of HcJps1 (**Fig. 3B**). Our experiments therefore suggest that the HcJps1 ortholog is able to adopt both a mono- and a dimeric state, which likely depend on the protein concentration. To assess whether the conserved core domain also forms a similar structural fold in SrJps1 and HcJps1, we predicted the structural models using AlphaFold2. Overall, the models share the architecture of UmJps1 and superpose well with RMSD of 0.8 (SrJps1) and 1.4 (HcJps1) over 287 and 136 Cα-atoms, respectively within the central core domain (**Fig. S7**).

bioRxiv preprint doi: https://doi.org/10.1101/2024.02.29.582524; this version posted March 2, 2024. The copyright holder for this preprint (which was not certified by peer review) is the author/funder, who has granted bioRxiv a license to display the preprint in perpetuity. It is made available under aCC-BY-NC-ND 4.0 International license.

To analyze the functional conservation of the orthologs *in vivo*, we generated complementation strains in which we produced the protein versions as translational fusions with Gfp (SrJps1G, HcJps1G) in the *jps1* deletion strain. Both fusion proteins were produced in full-length as verified by western blotting (**Fig. S8A**). Biochemical *in vivo* studies revealed full complementation of extracellular Cts1 activity for the strain expressing SrJps1G (**Fig. 3C**). By contrast, no complementation was achieved by the short version HcJps1, and extracellular chitinase activity could not be detected (**Fig. 3C, S8**). Instead, intracellular Cts1 activity was increased in strains producing HcJps1G, suggesting that the protein remained and accumulated in the cells as observed for *jps1* deletion strains (**Fig. S8B**).

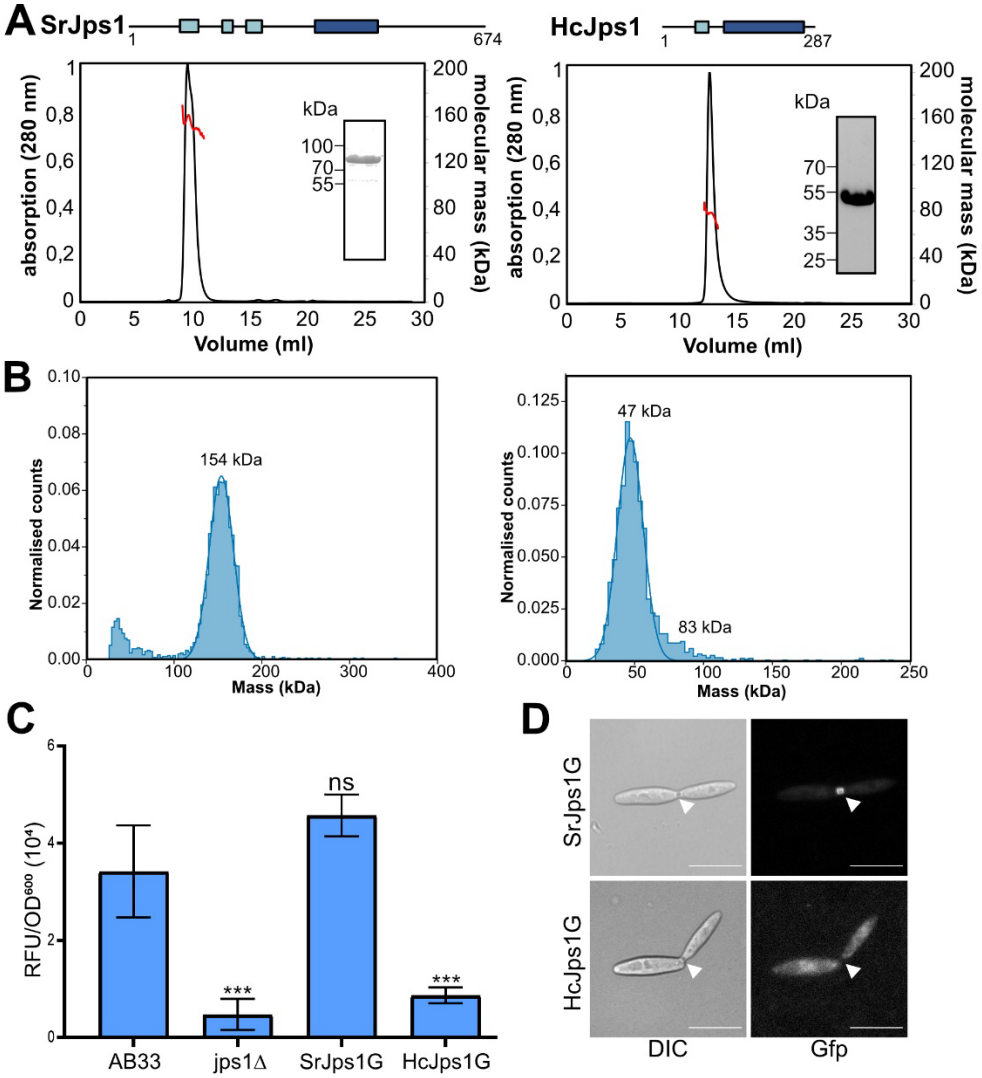

Figure 3: Biochemical analysis of Jps1 orthologs confirms dimerization but reveals functional diversification. A. Schematic representation of SrJps1 (left) and HcJps1 (right) protein architecture. The conserved core domain is depicted as red box. SEC-MALS of full-length recombinant SrJps1 and HcJps1. The black line shows the absorption at 280 nm (SEC), the molecular weight as determined by MALS is depicted in red. The insets show SDS-PAGE of purified proteins before SEC-MALS. **B.** Mass photometry of SrJps1 (left) and HcJps1 (right) at 10 nM concentration. **C.** Extracellular Cts1 activity of indicated strains. AB33jps1Δ was used as negative control, the progenitor AB33 dealt as positive control. Error bars depict standard deviation. ***P-value 0.001; n.s., not significant (two sample t-test). **D.** Fluorescence microscopic localization of SrJps1-G and HcJps1-G in the complementation strains. DIC, differential interference contrast. Scale bars, 10 µm.

bioRxiv preprint doi: https://doi.org/10.1101/2024.02.29.582524; this version posted March 2, 2024. The copyright holder for this preprint (which was not certified by peer review) is the author/funder, who has granted bioRxiv a license to display the preprint in perpetuity. It is made available under aCC-BY-NC-ND 4.0 International license.

Accordingly, fluorescence microscopy using the respective strains revealed a localization of SrJps1G but not HcJps1 in the fragmentation zone (**Fig. 3D**). In summary, the characterization of Jps1 orthologs confirmed the conservation of the dimerization via the core domain. Our complementation studies further suggest that Jps1 has functionally diversified in more distantly related basidiomycete species, resulting in the correct subcellular localization of the *S. reilianum* ortholog but not the one from *H. cylindrosporum.*

Jps1 interacts with phosphatidylinositol phosphates

Jps1 localizes in the membrane-rich fragmentation zone and particularly accumulates at the membrane enclosing the small compartment which is likely derived from the plasma membrane (Weinzierl, Leveleki et al. 2002, Reindl, Hansch et al. 2019). This membrane localization could either be mediated through a direct lipid interaction or indirect via interaction with a yet unknown factor. To test these two scenarios, we used our purified recombinant Jps1 to screen for membrane affinity using commercially available PIP strips (Echelon Biosciences Inc.) in lipid-protein interaction assays. Interactions of varying strengths were detected when Jps1 was incubated with the PIP strip membrane, including all phosphatidylinositol phosphates (PIP) and phosphatidic acid (PA; **Fig. S9A**). To corroborate this membrane binding, we generated heavy liposomes containing DOPC, the varying phospholipids or PA, and eventually cholesterol and performed interaction assays by mixing the liposomes with recombinant protein followed by high-speed centrifugation. The recombinant NADPH oxidase p40 (PX) domain of *U. maydis* Yup1 (Wedlich-Soldner, Bolker et al. 2000) was used as a positive control known to bind PI3P (**Fig. S9B**). While Jps1 did not bind to pure DOPC liposomes or liposomes containing PA, we detected weak binding to all PIPs except for PI(3,4,5)P_3 and to cholesterol. In some cases, like for PI(3,4)P_2 and PI(5)P the addition of cholesterol slightly increased the binding to the PIPs (**Fig. S9C**). Overall, we did not observe strong PIP binding and also noted degradation of Jps1 during our assays. We therefore decided to test, whether the previously characterized orthologs SrJps1 and HcJps1 could be used for the liposome assays instead. SrJps1 behaved similarly to UmJps1 but showed stronger binding to PI(4,5)P_2 compared to the other used PIPs (**Fig. S9D**). A substantial subfraction of HcJps1 bound to PI(4,5)P_2 liposomes in both the absence and even better in the presence of cholesterol. In the case of PI(4)P, a slightly weaker binding to the liposomes was detected (**Fig. S9E**). Overall, our results therefore suggested that Jps1 preferentially binds to PI(4,5)P_2, while instability of UmJps1 and SrJps1 resulted in a less stringent binding behavior.

For verification, we generated giant unilamellar vesicles (GUVs) containing cholesterol and PI(4,5)P_2 or PI(3,4,5)P_3. Recombinant Jps1 fused to Gfp (Jps1G) and Gfp as a negative control purified from *E. coli* was incubated with the GUVs and interaction was visualized by

bioRxiv preprint doi: https://doi.org/10.1101/2024.02.29.582524; this version posted March 2, 2024. The copyright holder for this preprint (which was not certified by peer review) is the author/funder, who has granted bioRxiv a license to display the preprint in perpetuity. It is made available under aCC-BY-NC-ND 4.0 International license.

fluorescence microscopy. While no interaction was detected for PI(3,4,5)P_3, a strong and stable association of Jps1G was obtained for PI(4,5)P_2 containing GUVs (**Fig. 4A**).

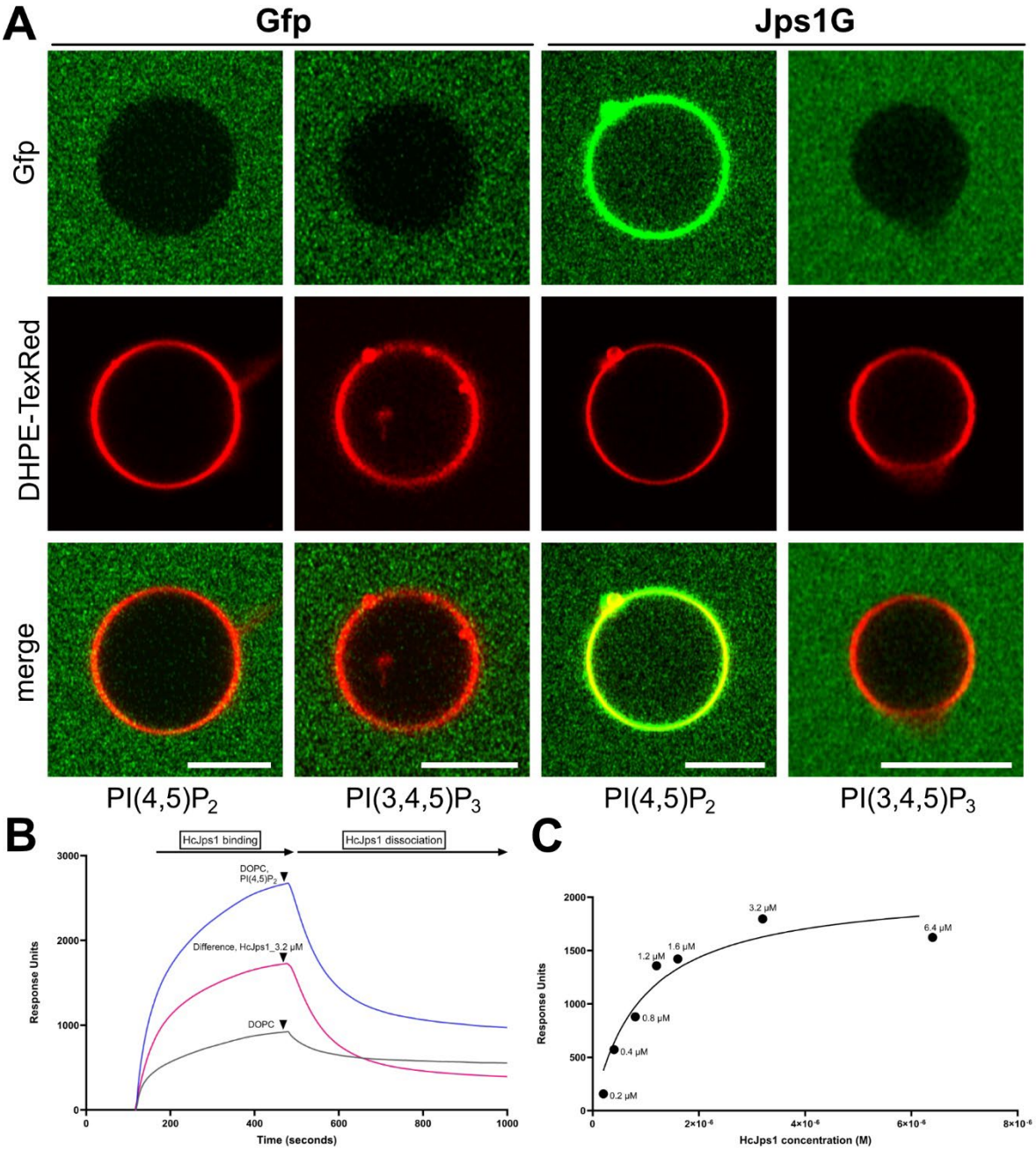

Figure 4: Liposome- and GUV-binding studies verifies Jps1 affinity to PI(4,5)P_2. A. Microscopic visualization of interaction of Jps1 with GUVs. GUVs containing the indicated PIPs were incubated with recombinant Jps1 fused to Gfp (Jps1G). Recombinant Gfp was used as a negative control, DHPE-TexRed was employed to stain vesicle membranes. **B.** Surface Plasmon Resonance (SPR) of HcJps1 at concentrations 0.2 to 6.4 µM binding to immobilized liposomes, followed by dissociation phase. Liposomes containing DOPC, PI(4,5)P_2 at 1 mM were used. DOPC-only liposome were used a negative control in the reference channel. **C**. Surface Plasmon Resonance (SPR) of HcJps1 at 3.2 µM indicating binding to the test liposomes DOPC, PI(4,5)P_2 shown as the difference between the test and the reference channel (DOPC-only liposomes).

To further characterize phosphoinositide binding, we performed quantitative analyses by surface plasmon resonance spectroscopy (SPR) using hydrophobic sensor chips with attached

bioRxiv preprint doi: https://doi.org/10.1101/2024.02.29.582524; this version posted March 2, 2024. The copyright holder for this preprint (which was not certified by peer review) is the author/funder, who has granted bioRxiv a license to display the preprint in perpetuity. It is made available under aCC-BY-NC-ND 4.0 International license.

PI(4,5)P_2^-containing liposomes and different concentrations of purified Jps1. While the interaction of UmJps1 with liposomes was difficult to address likely due to aggregation on the chip, we could confirm the specific interaction of HcJps1 with PI(4,5)P_2 containing liposomes (1 mM) at concentrations between 0.2 and 6.4 µM, after which the response units reached the saturation level (**Figs. 4B, C, S10**). The measurements obtained in this concentration range provided an estimate of the dissociation constant K_D for HcJps1:PI(4,5)P_2 interactions to be 0.9 µM (900 nM). This notably signifies that HcJps1 displays a strong binding affinity to PI(4,5)P_2. In essence, Jps1 displays PIP binding activity that likely mediates membrane attachment with specificity for PI(4,5)P_2-rich membranes. Importantly, PI(4,5)P_2 is characteristic for the inner leaflet of the plasma membrane (De Craene, Bertazzi et al. 2017). We therefore provide strong evidence that Jps1 dimers are targeted to the zone of unconventional secretion by a direct interaction with the specific lipid of the membrane, support our hypothesizes that Jps1 interacts directly with this membrane in the fragmentation zone.

bioRxiv preprint doi: https://doi.org/10.1101/2024.02.29.582524; this version posted March 2, 2024. The copyright holder for this preprint (which was not certified by peer review) is the author/funder, who has granted bioRxiv a license to display the preprint in perpetuity. It is made available under aCC-BY-NC-ND 4.0 International license.

Discussion

In recent years, different unconventional secretion mechanisms have been described in eukaryotes that deliver a variety of target cargo to the plasma membrane and beyond (Rabouille 2017, Dimou and Nickel 2018, Nickel and Rabouille 2018). We have previously reported a new type of unconventional secretion mechanism underlying export of the chitinase Cts1 in *Ustilago maydis* (Stock, Sarkari et al. 2012, Reindl, Hansch et al. 2019). We furthermore identified the protein Jps1 as important factor for this secretion mechanism while lacking detailed insights (Reindl, Stock et al. 2020, Philipp, Hussnaetter et al. 2021). Here, we therefore combined biochemical and *in vivo* experiments to investigate how Jps1 contributes to this export mechanism. Our findings reveal that Jps1 directly targets the membrane through an intrinsic affinity to PIPs, particularly to PI(4,5)P_2. A combination of biochemical and biophysical techniques furthermore demonstrated that Jps1 is a flexible and highly dynamic protein that homodimerizes through a conserved structural domain. Thus, our findings not only allow to refine the model of unconventional secretion of Cts1 in *U. maydis* but also expand our current knowledge on unconventional secretion mechanisms.

Expanding the model of unconventional secretion in *Ustilago maydis* and beyond

The recruitment of homodimeric Jps1 to the fragmentation zone, mediated by interaction with the PI(4,5)P_2-rich inner leaflet of the plasma membrane, supports the hypothesis that Jps1 serves as a tether for Cts1 accumulation at the site of cell separation (**Fig. 5**). In line with that, we see a slight interaction of Jps1 and Cts1 in yeast-two hybrid assays and Cts1 is excluded from the fragmentation zone in the absence of Jps1 (Reindl, Stock et al. 2020). The precise Cts1 interaction interface at Jps1 has not been clarified yet. However, the expanded structural architecture of the Jps1 homodimer offers ample possibilities for protein:protein interactions. Truncating the conserved core domain of Jps1 diminishes extracellular chitinase activity (Reindl, Stock et al. 2020), suggesting that Cts1 interaction is either mediated by this part of the protein or homodimerization is a prerequisite for proper function of Jps1. The process of unconventional Cts1 secretion might also involve other factors that interact with Jps1 and require the presence of the structural domains. Such protein:protein interactions could also be critical to determine the specificity of binding PIPs in the fragmentation zone but not in the mother or daughter cell. This hypothesis is further supported by the poor sequence conservation in Jps1 orthologs apart from the core domain.

bioRxiv preprint doi: https://doi.org/10.1101/2024.02.29.582524; this version posted March 2, 2024. The copyright holder for this preprint (which was not certified by peer review) is the author/funder, who has granted bioRxiv a license to display the preprint in perpetuity. It is made available under aCC-BY-NC-ND 4.0 International license.

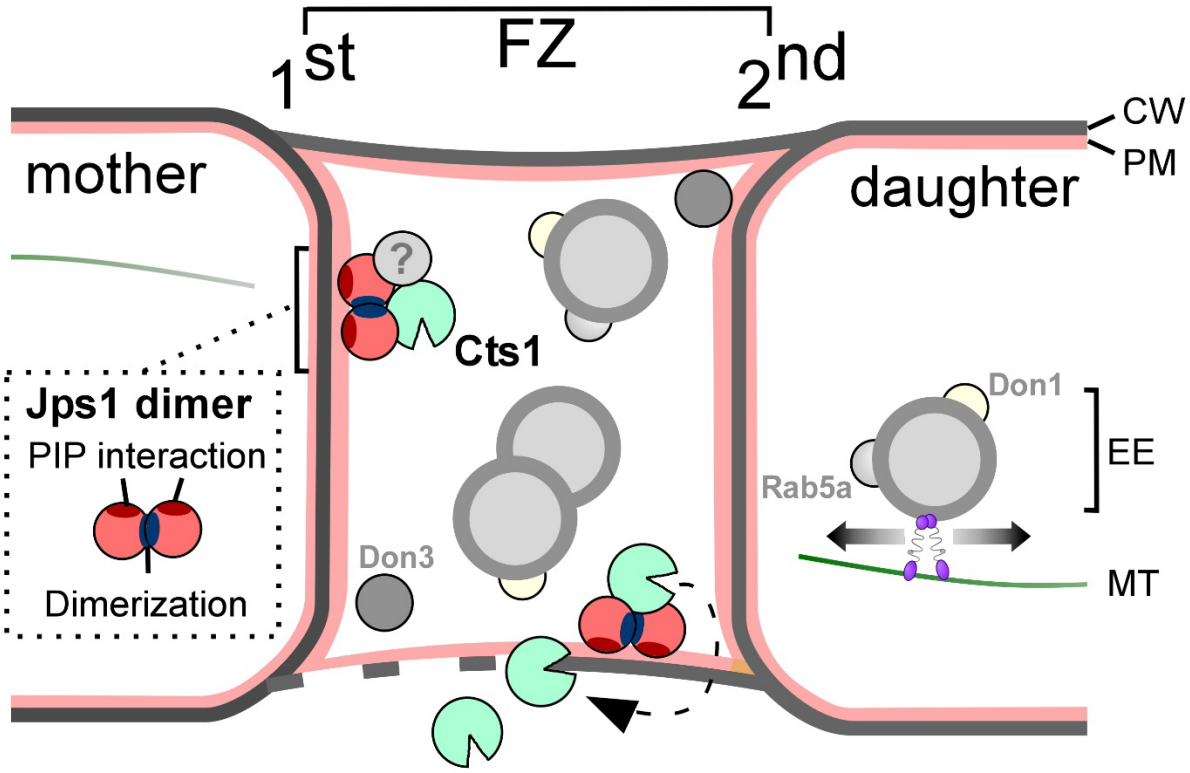

Figure 5. Schematic model of cytokinesis-dependent unconventional secretion. The picture shows the fragmentation zone (FZ) between two dividing yeast cells that is delimited by the primary (1st) and secondary septum (2nd). The fragmentation zone is completely encased by a peripheral membrane that is likely derived from the plasma membrane (PM). Jps1 and Cts1 both accumulate in the fragmentation zone. The former acts as a (homo)dimer and presumably interacts with the PIP PI(4,5)P_2 of the peripheral membrane. Our data support the hypothesis that Jps1 recruits chitinase Cts1 to the FZ. After secretion, the chitinase supports cell division by hydrolyzing remnant chitin. The fragmentation zone also contains early endosomes (EE) that shuttle bidirectionally throughout the yeast cells and accumulate in the FZ. Motile EE carry the proteins Rab5a and the GEF Don1. Kinase Don3 resides in the FZ. CW, cell wall; MT, microtubules.

In the course of this investigation, we therefore also explored a potential functional conservation of Jps1 orthologs within the phylum of basidiomycetes. Jps1 of *S. reilianum*, a very close dimorphic relative and a pathogen of corn and sorghum (Poloni and Schirawski 2016), shows high sequence conservation as well as complete functional complementation and a similar biochemical behavior. By contrast, the other – more distant – ortholog from *H. cylindrosporum* shares biochemical key features like dimerization and PI(4,5)P_2 affinity while functional complementation *in vivo* is lost. The strong reduction in protein size for this ortholog suggests that the protein has undergone evolutionary adaptations to its lifestyle. Interestingly, *H. cylindrosporum* is a mushroom-forming, hyphal fungus and yeast-like growing stages are not described (Marmeisse, Guidot et al. 2004). In the filamentous form of *U. maydis*, Cts1 localizes to the growth apex as well as to retraction septa and the cell wall of empty sections, suggesting an involvement in degradation of remnant chitin in dead hyphal parts (Langner,

bioRxiv preprint doi: https://doi.org/10.1101/2024.02.29.582524; this version posted March 2, 2024. The copyright holder for this preprint (which was not certified by peer review) is the author/funder, who has granted bioRxiv a license to display the preprint in perpetuity. It is made available under aCC-BY-NC-ND 4.0 International license.

Ozturk et al. 2015). Septal localization is in line with the idea of septum-directed secretion described for *Aspergillus oryzae* (Hayakawa, Ishikawa et al. 2011), where classical secretion via exocytosis occurs not only towards the cell exterior but also towards the septal membrane. We speculate that this phenomenon is not restricted to proteins with a canonical signal peptide but also occurs in alternative secretion routes. In this respect it is interesting to note that a glycoside hydrolase 18 (GH18) domain chitinase lacking a predicted signal peptide is present also in *H. cylindrosporum*. However, future research will have to address whether a similar mechanism of unconventional secretion exists in *H. cylindrosporum*.

In conclusion, we demonstrate that the direct PIP interaction crucial for unconventional secretion of Cts1 in *U. maydis*, is conserved across basidiomycete Jps1 orthologs, although their precise functional roles might have diversified.

Direct interaction with membranes via PIP binding is crucial for unconventional secretion

Multiple experimental evidence has demonstrated that Jps1 has an affinity to PIPs, particularly to PI(4,5)P_2. This phosphoinositide mainly localizes to the cytoplasmic leaflet of the plasma membrane dealing as a landmark for recruitment of cytosolic proteins and involved in regulating the activity of integral membrane proteins (Falkenburger, Jensen et al. 2010). It is crucial for important cellular processes including membrane fusion, signal transduction and also protein translocation (Balla 2013). Various phosphoinositide binding protein domains have been described in literature, including Pleckstrin-homology domain (PH) mediating binding to various PIPs, Phox-homology (PX) and FYVE zinc finger domains interacting specifically with PI3P (Stahelin, Scott et al. 2014). All of these domains have a conserved three-dimensional fold that provides the structural scaffold for residues recognizing the phosphate moieties of different phosphoinositides. In Jps1 we do not see obvious similarities to any of the described phosphoinositide binding domains, suggesting the absence of a structured binding domain. However, besides distinct domains also polybasic stretches can support PIP binding via electrostatic interactions (Gambhir, Hangyas-Mihalyne et al. 2004). Hence, we assume that a cluster of basic, positively charged residues (lysine, arginine) distributed across the Jps1 sequence might get in proximity in the folded protein to mediate PI(4,5)P_2 binding. Although Jps1 has several regions of high flexibility, our SAXS analysis suggests that they rather adopt a compact conformation and align to the central core domain (**Fig. 1D**). We therefore consider it possible that PIP-binding is mediated by residues within these flexible regions, which might even become more rigid in the presence of a bound PIP.

bioRxiv preprint doi: https://doi.org/10.1101/2024.02.29.582524; this version posted March 2, 2024. The copyright holder for this preprint (which was not certified by peer review) is the author/funder, who has granted bioRxiv a license to display the preprint in perpetuity. It is made available under aCC-BY-NC-ND 4.0 International license.

The interaction with PIPs, particularly with PI(4,5)P_2, is a phenomenon also observed in distinct other pathways of unconventional secretion where proteins are secreted via direct translocation (type I unconventional protein secretion). The detailed insights available for the export of the mammalian FGF2, for example, demonstrate that the protein oligomerizes at the inner leaflet of the cytoplasmic membrane via PI(4,5)P_2 interaction and this process is essential for secretion (Temmerman, Ebert et al. 2008, Steringer and Nickel 2018). Interestingly, also in this case a canonical PIP binding domain is absent while a stretch of three basic residues exposed at the protein surface is responsible for PI(4,5)P_2 interaction (Temmerman, Ebert et al. 2008). Isothermal titration calorimetry measurements showed a binding affinity with a K_d of about 0.5 µM for the PI(1,4,5)$_3$ head group, which is in the molar range of our results obtained in SPR measurements with recombinant HcJps1. Similar export mechanisms were proposed for other important mammalian proteins like IL-1β or Tau and viral HIV-Tat, and all depend on membrane recruitment via PI(4,5)P_2 (Zeitler, Steringer et al. 2015, Brough, Pelegrin et al. 2017, Katsinelos, Zeitler et al. 2018). Further proteins that are unconventionally secreted and rely on PI(4,5)P_2 binding for export are homeodomain proteins like Engrailed-2 (EN2), acting as important spatial determinants of body plan development in humans. Similar to our observations with Jps1, a supporting role of cholesterol for interaction with PI(4,5)P_2 been described also for FGF2 and EN-2, however, the underlying mechanistic details are not yet understood (Joliot 2023). Thus, albeit the molecular mechanism of membrane translocation is completely unknown for Jps1, its intriguing to note that PI(4,5)P_2 and cholesterol binding seem to constitute a key feature that is conserved between unconventional secretion pathways of yeast and mammalian cells.

In essence, our study revealed the first detailed insights into the function of Jps1 during unconventional Cts1 secretion and specifically underpins the important role of phosphoinositide interaction for these alternative export pathways.

bioRxiv preprint doi: https://doi.org/10.1101/2024.02.29.582524; this version posted March 2, 2024. The copyright holder for this preprint (which was not certified by peer review) is the author/funder, who has granted bioRxiv a license to display the preprint in perpetuity. It is made available under aCC-BY-NC-ND 4.0 International license.

Experimental procedures

Accession numbers

The genes and encoding protein sequences are available from Uniprot (https://uniprot.org) with the following accession numbers: *U. maydis* Jps1 (A0A0D1C3B2), *S. reilianum* Jps1 (A0A2N8UGD0), *H. cylindrosporum* Jps1 (A0A0C3CFZ0).

Molecular cloning and strain generation

Escherichia coli Top10 cells (Invitrogen) were used for cloning purposes. Gibson assembly and Golden Gate cloning strategies adapted for efficient generation of plasmids for protein production in *E. coli* and genetic modification of *U. maydis* were employed (Gibson, Young et al. 2009, Terfruchte, Joehnk et al. 2014, Zweng, Mendoza-Rojas et al. 2023). All plasmids were verified by restriction analysis and sequencing. All oligonucleotides used in this study are listed in Table S2.

Plasmids for protein production in *E. coli* were based on pET22b or pEMGB1 (Table S3). The generation of the plasmid pET22b_Jps1_6xHis (pUMa3257) was done using the oligonucleotides oMB945 and oMB946 for amplification of *jps1* from genomic DNA of the sequenced *U. maydis* strain UM521 (Table S3). For generation of the plasmids pEMGB1_Jps1_1-218 (pUX84), pEMGB1_Jps1_1-484 (pUX85), pUMa3257 was used for the amplification of respective *jps1* gene regions. Subsequently, the backbone of pEMGB1_mScarlet (pIL17) (Zweng, Mendoza-Rojas et al. 2023) was used for *Bsa*I mediated Golden Gate cloning and respective amplified genes were inserted into it. Similarly, genes encoding Jps1 orthologs were cloned into pEMGB1 backbone. *S. reilianum* genomic DNA was isolated from the strain *Sporisorium reilianum* SRZ2 (CBS 131459) (Kellner, Vollmeister et al. 2011) and used as template for PCR reactions with the described oligonucleotides to amplify *S. reilianum jps1* gene, which was then further cloned into pEMGB1 backbone to obtain pEMGB1_SrJps1 (pUX91). The gene sequence of *H. cylindrosporum jps1* was dicodon optimized for expression in *U. maydis* (Zhou, Obhof et al. 2018) and ordered as a gBlock (Integrated DNA Technology, Coralville, Iowa, United States). The optimized sequence was used as a template for PCR reactions with the described oligonucleotides to generate *H. cylindrosporum jps1* gene, which was then further cloned into pEM-GB1 to obtain pEMGB1_HcJps1 (pUX122).

Plasmids for genetic modification in *U. maydis* contained a resistance cassette for selection and flanking regions of about 1 kb for homologous recombination, yielding stable strains. For generation of complementation strains, initially the backbone of pPjps1_ Jps1_eGfp_CbxR (pUMa3293) (Reindl, Stock et al. 2020) was used to generate pPjps1_Jps1_eGFP_nosT_T2857A_ CbxR (pUX168) based on site-directed mutagenesis to eliminate a EcoRI site. This plasmid was then hydrolyzed with BamHI and EcoRI to be used as a vector backbone for generating plasmids pPjps1_SrJps1_eGfp_CbxR (pUX169), pPjps1_HcJps1_eGfp_CbxR (pUX171), pPjps1_Jps1_1-484_eGfp_CbxR (pUX172). The respective *jps1* genes in these plasmids were amplified using Gibson Assembly oligonucleotides as described in the Table S2. Linear constructs obtained by hydrolysis of the respective plasmids were used to transformation *U. maydis* laboratory strain AB33 or derivatives (Brachmann, Weinzierl et al. 2001). Genetic modifications were verified by Southern blot analysis using the flanking regions as probes. All *U. maydis* strains, genotypes and plasmids used for genetic engineering are listed in Table S4.

Cultivation

U. maydis strains were grown at 28°C in complete medium (CM) supplemented with 1% (w/v) glucose (CM-glc) using baffled flasks and constant shaking at 200 rpm (Holliday

bioRxiv preprint doi: https://doi.org/10.1101/2024.02.29.582524; this version posted March 2, 2024. The copyright holder for this preprint (which was not certified by peer review) is the author/funder, who has granted bioRxiv a license to display the preprint in perpetuity. It is made available under aCC-BY-NC-ND 4.0 International license.

1974). Solid media were supplemented with 2% (w/v) agar. CM-glc agar plates were used for growing the strains on plates.

Determination of chitinase activity

For determination of extracellular chitinase activity, liquid assays were performed with intact cells according to published protocols (Koepke, Kaffarnik et al. 2011, Stock, Sarkari et al. 2012). An overnight 5 mL CM-glc pre-pre-culture was grown at 28°C, followed by a pre-culture grown over the day. The main culture (10 mL) was then started from this pre-culture to reach an OD_{600} of 1.0 overnight. 2 mL culture was then harvested at 5,000 rpm for 5 min and the pellet was resuspended in 1 mL KHM buffer (110 mM potassium acetate, 20 mM HEPES, 2 mM $MgCl_2$). The OD_{600} of this suspension was documented for the analysis of data. 30 µL of each sample was transferred to a black 96-well plate (96 well, PS, F-Bottom, µCLEAR, black, CELLSTAR). MUC, a fluorogenic substrate 4-methylumbelliferyl-β-D-N, N', N''-triacetylchitotrioside (MUC, Sigma) (Langner, Ozturk et al. 2015) was dissolved in DMSO to obtain a stock of 2 mg/mL. The reaction was then initiated by adding 70 µL of MUC working solution containing MUC diluted with KHM buffer (1:10) to 30 µL of the samples. Fluorescence was determined at excitation/emission wavelengths of 360/450 nm at intervals of 5 min for 1 hour at 25°C using the Tecan Infinite M200 plate reader (Männedorf, Switzerland). The gain of the measurement was adjusted for each measurement (gain optimal). Obtained fluorescence values were normalized using OD_{600}. For determination of Cts1 activity in the cell extracts, the native cell extracts were prepared as mentioned in the section for Western blot analysis. The total protein concentration of these cell extracts was adjusted to 33 µg/mL using KHM buffer. 30 µL of each extract were then analyzed for Cts1 activity as per the protocol mentioned above.

Protein production and purification in *Escherichia coli*.

E. coli BL21 (DE3) (Invitrogen/Life Technologies) and Rosetta(DE3)pLyS cells (Novagen, Merck Millipore) were transformed with plasmid of interest to produce proteins fused with an N-terminal hexa-histidine (His) tag or proteins carrying both GB1 and His-tag. Transformed cells were grown on dYT-agar plates supplemented with 100 µg/mL ampicillin for *E. coli* BL21(DE3) and with 100 µg/mL ampicillin and 34 µg/mL chloramphenicol for Rosetta (DE3)pLyS. Colonies from the plate were used to inoculate a pre-culture in 100 mL dYT medium with appropriate antibiotics grown for 16 h at 37°C under constant shaking at 200 rpm. According to the requirements of the protein of interest, the induction was done either by 1% (w/v) lactose or 0.5 mM isopropyl-β-D-1-thio-galactopyranoside (IPTG, Sigma Aldrich) (**Table 1**). For lactose induction, the main culture was inoculated and subsequently grown at 30 °C for 20 h at 200 rpm. For IPTG induction, a preculture was inoculated and grown at 37°C for 12-16 h which was then used to start a main culture at OD_{600} 0.1, incubated until the OD_{600} reached 0.6. The cultures were then cooled down to 20 °C and protein production was induced by adding 0.5 mM IPTG. The cells continued to grow for 20 h at 20°C and 200 rpm. The cultures were harvested by centrifugation (4,000 g, 15 min, 4°C), resuspended in buffer A (20 mM HEPES pH 8, 20 mM KCl, 40 mM imidazole and 250 mM NaCl) and subsequently disrupted using a microfluidizer (M110-L, Microfluidics). The cell debris was removed by centrifugation (50,000 g, 20 min, 4 °C). The supernatant was loaded onto Ni-NTA FF-HisTrap columns (Cytiva) for affinity purification via the His-tag. The columns were washed with buffer A (10x column volume) and eluted with buffer B (20 mM HEPES pH 8, 20 mM KCl, 250 mM imidazole and 250 mM NaCl). Eventually, prior to size-exclusion chromatography (SEC), the GB1-tag was cleaved off by adding 0.4 mg TEV protease directly to the eluate and incubating under constant rotation at 20°C for 3 h. Cleaved His-tagged GB1 fragment and remaining TEV were

bioRxiv preprint doi: https://doi.org/10.1101/2024.02.29.582524; this version posted March 2, 2024. The copyright holder for this preprint (which was not certified by peer review) is the author/funder, who has granted bioRxiv a license to display the preprint in perpetuity. It is made available under aCC-BY-NC-ND 4.0 International license.

removed via a second Ni-NTA purification after buffer exchange to buffer A using an Amicon Ultra-10K centrifugal filter (Merck Millipore). The tag-free protein was subjected to SEC using a Superdex 200 Increase 26/600 column equilibrated in HEPES buffer (20 mM HEPES pH 7.5, 20 mM KCl and 200 mM NaCl). The peak fractions were analyzed using a standard SDS-PAGE protocol, pooled, and concentrated with Amicon Ultra-10/30/50K centrifugal filters.

Table 1. Specific induction conditions for the different recombinant proteins produced in *E. coli*.

Protein	*E. coli* strain used	Induction conditions	Buffer used for purification	Usage
6xHis-Jps1	Rosetta(DE3) pLyS	0.5 mM IPTG, 18°C/18 h	HEPES Buffer	MALS, mass photometry, lipid-binding assays
6xHis-GB1-Jps1$^{1-484}$	Rosetta(DE3) pLyS	1% lactose (w/v), 30°C/20 h	HEPES Buffer	MALS, mass photometry, lipid-binding assays, SAXS analysis
6xHis-GB1-Jps1$^{1-218}$	Rosetta(DE3) pLyS	0.5 mM IPTG, 37°C/3 h	HEPES Buffer	MALS, mass photometry, lipid-binding assays
6xHis-GB1-SrJps1	BL21(DE3)	1% lactose (w/v), 30°C/20 h	HEPES Buffer	MALS, mass photometry, lipid-binding assays
6xHis-GB1-HcJps1	BL21(DE3)	1% lactose (w/v), 30°C/20 h	HEPES Buffer	MALS, mass photometry, lipid-binding assays

Multi-angle light scattering

MALS was performed after SEC purification of the protein of interest. The collected sample was applied onto another SEC column (Superdex 200 GL 10/30; GE Healthcare) which was directly connected to a triple-light scattering detector (miniDAWN TREOS, Wyatt Technology Europe GmbH, Dernbach, Germany) and a differential refractive index detector (OPTILab T-rEX, Wyatt Technology). Astra7 (Wyatt Technology) was used for evaluation of the collected data.

Mass photometry

Mass photometry experiments were performed using a TwoMP mass photometer (Refeyn Ltd, Oxford, UK). Data acquisition was performed using AcquireMP (Refeyn Ltd. v2.3). Mass photometry movies were recorded at 1 kHz, with exposure times varying between 0.6 and 0.9 ms, adjusted to maximize camera counts while avoiding saturation. Microscope slides (70 x 26 mm) were cleaned for 5 min in 50% (v/v) isopropanol (HPLC grade in Milli-Q H_2O) and pure Milli-Q H_2O, followed by drying with a pressurized air stream. Silicon gaskets to hold the sample drops were cleaned in the same manner and fixed to clean glass slides immediately prior to measurement. The instrument was calibrated using the NativeMark Protein Standard (Thermo Fisher Scientific) immediately prior to measurements. The concentration during measurement of UmJps1 full length and variants as well as Jps1 orthologs was typically 10 nM. Each protein was measured in a new gasket well (i.e., each well was used once). To find focus, 18 µL of fresh HEPES buffer adjusted to room temperature was pipetted into a well, the focal position was identified and locked using the autofocus function of the instrument. For each acquisition,

bioRxiv preprint doi: https://doi.org/10.1101/2024.02.29.582524; this version posted March 2, 2024. The copyright holder for this preprint (which was not certified by peer review) is the author/funder, who has granted bioRxiv a license to display the preprint in perpetuity. It is made available under aCC-BY-NC-ND 4.0 International license.

2 µL of diluted protein was added to the well and thoroughly mixed. For each sample, three individual measurements were performed. The data were analyzed using the DiscoverMP software.

Hydrogen/deuterium exchange mass spectrometry (HDX-MS)

HDX-MS samples were prepared by a two-arm autosampler (LEAP Technologies). Reactions were initiated by adding 58.5 µL of buffer prepared with D_2O (20 mM HEPES-Na pH 7.5, 20 mM KCl, 20 mM $MgCl_2$, 200 mM NaCl), to 6.5 µL of Jps1 solution (50 µM). After incubation at 25 °C for 10, 95, 1,000 or 10,000 s, HDX was quenched by transferring 55 µL of the reaction to another well containing 55 µL of 400 mM KH_2PO_4/H_3PO_4, 2 M guanidine-HCl (pH 2.2) kept at 1 °C. After mixing, 100 µL of the quenched reaction were injected into an ACQUITY UPLC M-Class system with HDX Technology (Wales, Fadgen et al. 2008). Non-deuterated samples were generated similarly with an H_2O-based buffer. The samples were washed from a 50-µL injection loop with water + 0.1% (v/v) formic acid (100 µL/min) and passed through a cartridge (2 mm x 2 cm, kept at 12 °C) filled with porcine pepsin immobilized to bead material. The resulting peptic peptides were collected on a trap column (2 mm x 2 cm; 0.5 °C) filled with POROS 20 R2 (ThermoFisher Scientific). After 3 minutes, the column was placed in line with an ACQUITY UPLC BEH C18 1.7 µm 1.0 x 100 mm column (Waters) temperated at 0.5 °C and the peptides eluted with a gradient of H_2O + 0.1% (v/v) formic acid (eluent A) and acetonitrile + 0.1% (v/v) formic acid (eluent B) at 60 µL/min, as follows: 0-9 min/95-55% A, 9-10 min/55-15% A, 10-10.1 min/15-5% A, 10.1-11/5% A. Peptides were guided to a Synapt G2-Si mass spectrometer (Waters) and ionized by electrospray ionization (capillary temperature: 250 °C; spray voltage: 3.0 kV). Mass spectra were acquired with MassLynX MS 4.1 (Waters) over 50 to 2,000 *m/z* in enhanced high-definition MS ($HDMS^E$) (Geromanos, Vissers et al. 2009, Li, Vissers et al. 2009) or high-definition MS (HDMS) mode for non-deuterated and deuterated samples, respectively. Lock-mass correction was conducted with [Glu1]-fibrinopeptide B standard (Waters). During peptide separation on the ACQUITY UPLC BEH C18 column, the pepsin column was washed 3 times with 80 µL of 0.5 M guanidine-HCl in 4% (v/v) acetonitrile. Blank runs (double-distilled H_2O) were performed between each sample. All measurements were performed in duplicate (separate HDX reactions).

Peptides were identified with ProteinLynx Global SERVER 3.0.1 (PLGS, Waters) from the non-deuterated samples acquired with $HDMS^E$ employing low-energy, elevated-energy and intensity thresholds of 300, 100 and 1,000 counts, respectively, and matched using a database containing the amino acid sequences of Jps1, porcine pepsin, and their reversed sequences (peptide tolerance = automatic; fragment tolerance = automatic; min fragment ion matches per peptide = 1; min fragment ion matches per protein = 7; min peptide matches per protein = 3; maximum hits to return = 20; maximum protein mass = 250,000; primary digest reagent = non-specific; missed cleavages = 0; false discovery rate = 100). For quantification of deuterium incorporation with DynamX 3.0 (Waters), peptides had to fulfil the following criteria: identification in both non-deuterated samples; minimum intensity of 20,000 counts; maximum length of 40 residues; minimum number of two products; maximum mass error of 25 ppm; retention time tolerance of 0.5 minutes. All spectra were manually inspected and omitted, if necessary, e.g., for low signal-to-noise ratios or overlapping peptides prohibiting correct assignment of the isotopic clusters.

Residue-specific deuterium uptake from peptides identified in the HDX-MS experiments was calculated with the software DynamX 3.0 (Waters). In the case that any residue is covered by a single peptide, the residue-specific deuterium uptake is equal to that of the whole peptide. In the case of overlapping peptides for any given residue, the residue-specific deuterium uptake is determined by the shortest peptide covering that residue. Where multiple peptides are of the

bioRxiv preprint doi: https://doi.org/10.1101/2024.02.29.582524; this version posted March 2, 2024. The copyright holder for this preprint (which was not certified by peer review) is the author/funder, who has granted bioRxiv a license to display the preprint in perpetuity. It is made available under aCC-BY-NC-ND 4.0 International license.

shortest length, the peptide with the residue closest to the peptide C-terminus is utilized. Assignment of residues exhibiting no higher-order structure (disordered) was based on two criteria, i.e., a residue-specific deuterium uptake of >50% after 10 s of HDX and no increment in HDX >5% in between consecutive HDX time-points (Goretzki, Wiedemann et al. 2023). Raw data of deuterium uptake by peptides and residue specific HDX are provided in **Supplementary Dataset 1** (Masson, Burke et al. 2019).

Small-angle X-ray scattering

SEC-SAXS data were collected on the P12 beamline (PETRA III, DESY Hamburg (Blanchet, Spilotros et al. 2015)). The sample to detector distance of the P12 beamline for was 3.00 m, resulting in an achievable q-range of 0.03 – 4.4 nm^{-1}. The measurement was performed at 10°C with a protein concentration of 0.6 mg/mL of purified $Jps1^{1-484}$. The sample was measured in batch mode and injected via autosampler. We collected 40 frames with an exposer time of 0.095 sec/frame. Data were collected on absolute scale intensity against water.

All used programs for data processing were part of the ATSAS Software package (Version 3.0.5) (Manalastas-Cantos, Konarev et al. 2021). Primary data reduction was initially performed with the SASFLOW (Franke, Kikhney et al. 2012) pipeline and checked with the programs PRIMUS (Konarev, Volkov et al. 2003). The Guinier approximation (Guinier 1939) was used to determine the forward scattering *I(0)* and the radius of gyration (R_g). The pair-distribution function *p(r)* was created with the program GNOM (Svergun 1992) and determined the maximum particle dimension (D_{max}). The rigid body modelling of the $Jps1^{1-484}$ dimer was done with CORAL (Petoukhov, Franke et al. 2012). We used an AlphaFold2 (Jumper, Evans et al. 2021, Mirdita, Schutze et al. 2022) prediction as template, where the flexible loop regions (aa 357-447) as well as the N-terminal residues (aa 1-17, 75-172) of the dimer were remodeled via CORAL (Petoukhov, Franke et al. 2012).

PIP overlay assays

The lipid binding analysis of Jps1 was performed using PIP Lipid Strips (Echelon Biosciences Inc.). Prior to their use, the lipid strips were blocked for one hour in 1x TBS buffer with 0.05 % Tween 20 (TBS-T) supplemented with 3 % (w/v) BSA. 5 µg of purified Jps1 protein was incubated with the pre-blocked strips in TBS-T buffer supplemented with 3% BSA in the dark (total volume 15 mL). Next, unbound protein was removed in three 10 min washing steps with TBS-T. An anti-His- primary antibody (Sigma, 1:2,000) was incubated with the protein-treated lipid strips to detect Jps1 bound via its C-terminal His-tag. The unbound antibody was then removed by subsequent washing steps after incubation. AceGlow Western Blot detection solution was used to detect chemiluminescent signals on the lipid membrane. 0.5 µg $PI(4,5)P_2$-grip protein (GST-tagged PLC-δ1 PH domain protein, Echelon) was used as positive control. Here, a primary anti-GST (Sigma, 1:3,000) was used to detect bound $PI(4,5)P_2$-grip protein.

Liposome binding assays

DOPC (1,2-di-(9Z-octadecenoyl)-sn-glycero-3-phosphocholine) (catalog no. 850375C-25MG), cholesterol (3β-hydroxy-5-cholesten, 5-cholesten-3β-ol) (catalog no. C8667-1G) and $PI(4,5)P_2$ (L-α-phosphatidylinositol-4,5-bisphosphate (Brain, Porcine) ammonium salt) (catalog no. 840046P-1MG) were purchased from Sigma Aldrich/Merck (manufactured by Avanti Polar Lipids, Inc.). Lipids solved in chloroform were mixed in desired concentrations and ratios, and chloroform was evaporated under vacuum conditions at 40°C using a rotary evaporator (IKA). The dried lipid film was then resuspended in 20 mM HEPES pH 7.5 buffer supplemented with 20 mM KCl and 200 mM NaCl to achieve the lipid concentration of 5 mM. In order to obtain large unilamellar vesicles, the crude liposomes were manually extruded through porous

bioRxiv preprint doi: https://doi.org/10.1101/2024.02.29.582524; this version posted March 2, 2024. The copyright holder for this preprint (which was not certified by peer review) is the author/funder, who has granted bioRxiv a license to display the preprint in perpetuity. It is made available under aCC-BY-NC-ND 4.0 International license.

polycarbonate membranes (Nucleopore, Whatman) using the Mini-Extruder set (Avanti Polar Lipids, Inc.). The membrane pore size was decreased stepwise from 200 nm to 50 nm. The control liposomes were prepared by using 100 mol % DOPC and DOPC / cholesterol in the molar ratio 80:20. Liposomes containing phosphoinositides were prepared by mixing DOPC:cholesterol:PIP and DOPC:PIP in the molar ratios 80:15:5 and 95:5, respectively.
For liposome binding assays, the protein of interest was mixed with liposomes in a protein: lipid molar ratio of 1:5,000 in a final volume of 100 µL made up with HEPES buffer (20 mM HEPES pH 7.5, 20 mM KCl and 200 mM NaCl). This suspension was incubated at room temperature for 15 min to allow the protein-liposome interaction. After incubation, the suspension was ultra-centrifuged at 52,000 rpm for 45 min. The pellet and supernatant fractions were then carefully separated and the pellet was resuspended in 100 µL HEPES buffer. The pellet and supernatant fractions were then precipitated by addition of 20% (w/v) TCA and further analyzed using standard SDS-PAGE protocol followed by Coomassie staining.

Binding studies using giant unilamellar vesicles

All lipids were purchased from Cayman Chemicals or Avanti Polar Lipids, and stock solutions (0.2 mg/mL, except for cholesterol 10 mg/mL) were prepared with chloroform. GUVs were produced using PVA-assisted swelling (Weinberger, Tsai et al. 2013). 100 µL of 5% (w/w) polyvinyl alcohol (PVA) were spread equally on the front of an object slide within a defined area. For drying, the PVA coated slide was placed on a thermoblock heated to 50°C. Lipids were mixed in the following molar ratios – DOPC (74.75 mol%), cholesterol (20 mol%), PIP (5 mol%), Texas Red (0.25 mol%). 10 µL of the lipid mixes were spread equally onto the PVA coated slides and another 10 µL was added upon the subsequent drying of the initial layer. Marked areas of PVA + dried lipids were surrounded by Vitrex on the slides in a “U”-shape. The second cleaned object slide was squeezed onto the Vitrex, generating a sealed chamber. Approximately, 500 µL of 10% (w/v) sucrose solution were filled carefully into the chamber. The sucrose-filled chamber was sealed at the top with another layer of Vitrex. Swelling was performed at room temperature (~25°C) for one hour. GUVs were harvested from the incubation chamber with microcapillary-tips (VWR) transferred into fresh reaction tubes and analyzed by microscopy.
For binding experiments, 10 µL of GUVs were used and mixed with different amounts of protein. 30-300 µg of 1 mg/mL purified Jps1G were used for the GUV binding studies. Total protein concentration in the well was adjusted with 1x TBS buffer (max. volume of plate wells: 50 µL). To immobilize GUVs and to avoid interaction of Jps1 with the negatively charged surface of the wells, Ibidi® plate wells were coated with 30 µL of β-casein solution for five minutes at room temperature. β-casein was discarded and wells were washed with 50 µL of 1xTBS-buffer three-times. These plates either coated with casein or uncoated were used for inverted laser scanning confocal microscopy with an AiryScan module (Zeiss).

Surface plasmon resonance (SPR)

The protein: lipid binding experiments were performed in the two-channel instrument 2SPR (AMETEK Reichert Inc., Depew, NY, USA) using SPR sensor chip LP (coating -lipophilic groups covalently bound to a 2D carboxymethyldextran surface) used for the capture of lipid membrane vesicles (XanTec bioanalytics GmbH, Düsseldorf, Germany). DOPC and DOPC, PI(4,5)P_2 liposomes were extruded respectively as mentioned before to the diameter of 50 nm. Initially, the chip surface was equilibrated with SPR running buffer (20 mM HEPES pH 7.5, 20 mM KCl and 200 mM NaCl) for 25 min. The chip was then cleaned simultaneously with 20 mM CHAPS (2 injections for 30s each), 50 mM NaOH (2 injections for 30 s each), 2:3 isopropanol:

bioRxiv preprint doi: https://doi.org/10.1101/2024.02.29.582524; this version posted March 2, 2024. The copyright holder for this preprint (which was not certified by peer review) is the author/funder, who has granted bioRxiv a license to display the preprint in perpetuity. It is made available under aCC-BY-NC-ND 4.0 International license.

50 mM NaOH (2 injections for 1 min each) at a flow rate of 25 µL*min^{-1}. The liposomes were immobilized at a flow rate of 10 µL*min^{-1} for 10 min to achieve 8,000 to 10,000 response units (RU). DOPC-only liposomes (1 mM) lacking the protein interaction were immobilized first in both the reference and test channel. The switch to the test channel was then made and the immobilized liposomes were removed completely using 2:3 isopropanol: 50 mM NaOH (1 injection for 1 min) until the response comes back to the baseline. After this, the DOPC, PI(4,5)P_2 (1 mM) liposomes were immobilized through the test channel. The switch to both channels was then made and 1 injection of 50 mM NaOH was done to remove any loosely bound liposomes. Further, BSA (0.5 mg/mL) was injected for 1 min to check the specificity of the liposomes. The flow rate was then switched to 25 µL*min^{-1} and the desired concentration of the protein of interest (200 µL) was injected. After each measurement, the chip was regenerated using the cleaning procedure mentioned above and further desired concentrations of protein were tested following the same procedure. Data was analysed using TraceDrawer (Version 1.9.2) software program (Ridgeview Instruments AB, Uppsala, Sweden). The data set was fitted by non-linear regression analysis of response units using the steady state affinity model:

$Y = B_{max} * c/ (c + K_D)$,

Where K_D is the dissociation constant, B_{max} is the maximum response unit, c is the concentration of HcJps1.

Western blot analysis

To evaluate the production of Jps1 variants in cell extracts, 50 mL cultures were grown to an OD_{600} of 1.0 and harvested at 5000 rpm for 5 min at 4°C. For intracellular Cts1 activity assays, the cell pellets were then resuspended in 1 mL of native extraction buffer containing 1X PBS pH 7.2, 100 µL 0.1 M PMSF (Sigma/Aldrich), 100 µL Protease inhibitor cocktail (Roche), 50 µL 0.5 mM benzamidine (Sigma Aldrich) and 400 µL of glass beads were added to each tube. The cells were then disrupted using Retsch Mill at 30 Hz for 15 min. After the cell disruption, the cell extracts were then centrifuged at 13,000 rpm for 30 min at 4°C to settle down the cell debris. The cell extracts were then transferred to fresh reaction tubes and used for further analysis. Alternatively, after harvesting the cultures, the cell pellets were resuspended in 2 mL PBS pH 7.2 and transferred to fresh centrifuge tubes. The cells were the harvested at 5,000 rpm for 5 min and the supernatant was removed completely. The resulting cell pellets were flash-frozen in liquid nitrogen, Sample tubes were placed on 24 well TissueLyser adapter Qiagen 69982) and soaked in liquid nitrogen for 1 min, followed by further addition of 5 mm stainless steel bead to each sample tube. The cells were disrupted using Retsch Mill at 30 Hz for 1 min X 3 cycles. After this, the dry homogenized powder of cells was resuspended in 1 mL urea buffer (8 M urea, 50 mM Tris/HCl pH 8.0 containing one tablet of ‘complete protease inhibitor” per 25 mL, 1 mM DTT, 0.5 mM benzamidine) and further centrifuged at 13,000 rpm for 10 minutes at 4°C. The supernatant was then used for subsequent analysis. Protein concentrations were determined by Bradford assay (BioRad, Hercules, CA, United States). 50 µg of total protein was analysed using standard SDS-PAGE protocol and transferred to a PVDF membrane (Amersham, Hybond -P), activated in 100% methanol using semi-dry Western blotting. Gfp-tagged protein of interest was detected using a primary mouse anti-Gfp (1:3,000, Millipore/Sigma). An anti-mouse IgG- horseradish peroxidase (HRP) conjugate (1:3,000 Promega) was used as secondary antibody. HRP activity was then detected using the Amersham ECL Primer Western Blotting Detection Reagent (Cytiva) and a LAS4000 chemiluminescence imager (GE Healthcare).

bioRxiv preprint doi: https://doi.org/10.1101/2024.02.29.582524; this version posted March 2, 2024. The copyright holder for this preprint (which was not certified by peer review) is the author/funder, who has granted bioRxiv a license to display the preprint in perpetuity. It is made available under aCC-BY-NC-ND 4.0 International license.

Microscopy

The microscopic analysis of an overnight grown culture (CM-glc) at OD_{600} of 0.5 was performed using wide-field fluorescence microscope Zeiss Axio Imager M1 equipped with a Spot Pursuit CCD camera (Diagnostic Instruments, Sterling Heights, MI) and objective lenses Plan Neofluar (63x, NA 1.25) and Plan Neofluar (100x, NA 1.40). The fluorescent proteins were excited with a HXP metal halide lamp (LEj, Jena) in combination with filter sets for Gfp (ET470/40BP, ET495LP, ET525/50BP), mCherry (ET560/40BP, ET585LP, ET630/75BP Chroma, Bellow Falls, VT), and DAPI (HC387/11BP, BS409LP, HC 447/60BP; AHF Analysentechnik, Tübingen, Germany). The system was operated by MetaMorph, version 7 (Molecular Devices, Sunnyvale, CA, United States). Image processing including the adjustments of brightness and contrast were conducted by ImageJ software version 1.54g.

Airyscan microscopy was applied using a Zeiss inverted LSM880 airyscan microscope system (Zeiss Microscopy GmbH, Oberkochen, Germany), equipped with a Plan-Apochromat 40x/1.2 water objective lens. Images were acquired using fast airyscan mode of the airyscan1 module. The general acquisition parameters were set as the following. 488 nm was used at 10% intensity as an excitation laserline for eGFP/Jps1-eGFP with a BP 465-505 + 525+555 nm detection filter. 561 nm was used at 1% intensity as an excitation laserline for the the TexasRed labeled GUVs with a BP 570-620 + LP 645 detection filter. The airyscan detector gain was set to 900 for eGFP/Jps1-eGFP and to 750 for TexasRed labeled GUVs. The scans were performed in unidirectional frame-sequential mode at a pixel dwell time of 0.98-1.96 µsec/pixel and a pixelsize of 99 nm. The final data were calculated using the Zeiss built in airyscan module and automatic ariyscan strength parameter were varying between 2.7-2.9 for eGFP/Jps1-eGFP and between 3.0-3.3 for TexasRed labeled GUVs.

Bioinformatics

For structure prediction of UmJps1 and orthologs, the respective sequences of the full-length proteins were downloaded from the UniProt database and AlphaFold2 v2.3 was used in Multimer mode using default settings (Jumper, Evans et al. 2021).

bioRxiv preprint doi: https://doi.org/10.1101/2024.02.29.582524; this version posted March 2, 2024. The copyright holder for this preprint (which was not certified by peer review) is the author/funder, who has granted bioRxiv a license to display the preprint in perpetuity. It is made available under aCC-BY-NC-ND 4.0 International license.

Data Availability

HDX-MS raw data are provided in the Supporting Information as Supplementary Dataset 1. We uploaded the SAXS data to the Small Angle Scattering Biological Data Bank (SASBDB) (Kikhney, Borges et al. 2020), with the accession codes SASDT97.

Author contributions

K.S. conceived of the project and designed the study. K.S, F.A. and S.D. wrote the paper with input from all other authors. S.D., M.S., M.Kö., M.Ka, M.B., W.S., S.H. and J.R performed experiments. S.D., M.S., W.S., J.R and F.A. analyzed data. S.S., A.K. and K.S. contributed funding and resources.

Supporting information

This article contains supporting information.

Acknowledgements

We are grateful to Bettina Axler for excellent technical support and Michael Feldbrügge for critical reading of the manuscript. We acknowledge the DESY (Hamburg, Germany), a member of the Helmholtz Association HGF, for the provision of experimental facilities. Parts of this research were carried out at PETRA III and we would like to thank Dmytro Soloviov (EMBL Hamburg) for the assistance in using beamline P12. We are grateful to Sebastian Joecks and Refeyn Ltd. for access to and assistance with the TwoMP mass photometer. We thank Eymen Hachani and Athanasios Papadopoulos from Biochemistry I at Heinrich-Heine University for conducting MALS analyses.

Funding and additional information

This work was funded by the German Research Foundation (DFG) within the Collaborative Research Center 1208 (project ID 267205415, sub-project A09/Schipper) and 1535 (project ID 458090666, sub-project Z01 to S.S. and J.R.). The Center for Structural studies is funded by the DFG (Grant number 417919780 and INST 208/761-1 FUGG to S.S.). We thank the German Research Foundation (DFG) for support through the Core Facility for Interactions, Dynamics and Macromolecular Assembly (project 324652314). We would like to acknowledge the Center for Advanced Imaging (CAi) at Heinrich-Heine-University Düsseldorf for providing access to the Zeiss LSM880 Airyscan system (Ref.No. DFG- INST 208/746-1 FUGG).

Conflict of Interest

The authors declare that they have no conflicts of interest with the contents of this article.

bioRxiv preprint doi: https://doi.org/10.1101/2024.02.29.582524; this version posted March 2, 2024. The copyright holder for this preprint (which was not certified by peer review) is the author/funder, who has granted bioRxiv a license to display the preprint in perpetuity. It is made available under aCC-BY-NC-ND 4.0 International license.

References

Altamirano, S., S. Chandrasekaran and L. Kozubowski (2017). "Mechanisms of Cytokinesis in Basidiomycetous Yeasts." Fungal Biol Rev **31**(2): 73-87.
Balla, T. (2013). "Phosphoinositides: tiny lipids with giant impact on cell regulation." Physiol Rev **93**(3): 1019-1137.
Blanchet, C. E., A. Spilotros, F. Schwemmer, M. A. Graewert, A. Kikhney, C. M. Jeffries, D. Franke, D. Mark, R. Zengerle, F. Cipriani, S. Fiedler, M. Roessle and D. I. Svergun (2015). "Versatile sample environments and automation for biological solution X-ray scattering experiments at the P12 beamline (PETRA III, DESY)." J Appl Crystallogr **48**(Pt 2): 431-443.
Brachmann, A., G. Weinzierl, J. Kamper and R. Kahmann (2001). "Identification of genes in the bW/bE regulatory cascade in Ustilago maydis." Mol Microbiol **42**(4): 1047-1063.
Brough, D., P. Pelegrin and W. Nickel (2017). "An emerging case for membrane pore formation as a common mechanism for the unconventional secretion of FGF2 and IL-1beta." J Cell Sci **130**(19): 3197-3202.
Cruz-Garcia, D., N. Brouwers, J. M. Duran, G. Mora, A. J. Curwin and V. Malhotra (2017). "A diacidic motif determines unconventional secretion of wild-type and ALS-linked mutant SOD1." J Cell Biol **216**(9): 2691-2700.
Cruz-Garcia, D., V. Malhotra and A. J. Curwin (2018). "Unconventional protein secretion triggered by nutrient starvation." Semin Cell Dev Biol **83**: 22-28.
De Craene, J. O., D. L. Bertazzi, S. Bar and S. Friant (2017). "Phosphoinositides, Major Actors in Membrane Trafficking and Lipid Signaling Pathways." Int J Mol Sci **18**(3).
Dimou, E. and W. Nickel (2018). "Unconventional mechanisms of eukaryotic protein secretion." Curr Biol **28**(8): R406-R410.
Duran, J. M., C. Anjard, C. Stefan, W. F. Loomis and V. Malhotra (2010). "Unconventional secretion of Acb1 is mediated by autophagosomes." J Cell Biol **188**(4): 527-536.
Falkenburger, B. H., J. B. Jensen, E. J. Dickson, B. C. Suh and B. Hille (2010). "Phosphoinositides: lipid regulators of membrane proteins." J Physiol **588**(Pt 17): 3179-3185.
Franke, D., A. G. Kikhney and D. I. Svergun (2012). "Automated acquisition and analysis of small angle X-ray scattering data." Nuclear Instruments and Methods in Physics Research Section A: Accelerators, Spectrometers, Detectors and Associated Equipment **689**: 52-59.
Gambhir, A., G. Hangyas-Mihalyne, I. Zaitseva, D. S. Cafiso, J. Wang, D. Murray, S. N. Pentyala, S. O. Smith and S. McLaughlin (2004). "Electrostatic sequestration of PIP2 on phospholipid membranes by basic/aromatic regions of proteins." Biophys J **86**(4): 2188-2207.
Geromanos, S. J., J. P. Vissers, J. C. Silva, C. A. Dorschel, G. Z. Li, M. V. Gorenstein, R. H. Bateman and J. I. Langridge (2009). "The detection, correlation, and comparison of peptide precursor and product ions from data independent LC-MS with data dependant LC-MS/MS." Proteomics **9**(6): 1683-1695.
Gibson, D. G., L. Young, R. Y. Chuang, J. C. Venter, C. A. Hutchison, 3rd and H. O. Smith (2009). "Enzymatic assembly of DNA molecules up to several hundred kilobases." Nat Methods **6**(5): 343-345.
Goretzki, B., C. Wiedemann, B. A. McCray, S. L. Schafer, J. Jansen, F. Tebbe, S. A. Mitrovic, J. Noth, A. C. Cabezudo, J. K. Donohue, C. M. Jeffries, W. Steinchen, F. Stengel, C. J. Sumner, G. Hummer and U. A. Hellmich (2023). "Crosstalk between regulatory elements in disordered TRPV4 N-terminus modulates lipid-dependent channel activity." Nat Commun **14**(1): 4165.
Guinier, A. (1939). "Small-angle X-ray diffraction: application to the study of ultramicroscopic phenomena." Annales de Physique **11**(12): 161-237.
Hayakawa, Y., E. Ishikawa, J. Y. Shoji, H. Nakano and K. Kitamoto (2011). "Septum-directed secretion in the filamentous fungus Aspergillus oryzae." Mol Microbiol **81**(1): 40-55.
Holliday, R. (1974). Ustilago maydis. Handbook of Genetics. **1:** 575-595.
Joliot, A. (2023). "Role of PI(4,5)P2 and Cholesterol in Unconventional Protein Secretion." Adv Exp Med Biol **1422**: 381-392.
Jumper, J., R. Evans, A. Pritzel, T. Green, M. Figurnov, O. Ronneberger, K. Tunyasuvunakool, R. Bates, A. Zidek, A. Potapenko, A. Bridgland, C. Meyer, S. A. A. Kohl, A. J. Ballard, A. Cowie, B. Romera-Paredes, S. Nikolov, R. Jain, J. Adler, T. Back, S. Petersen, D. Reiman, E. Clancy,

bioRxiv preprint doi: https://doi.org/10.1101/2024.02.29.582524; this version posted March 2, 2024. The copyright holder for this preprint (which was not certified by peer review) is the author/funder, who has granted bioRxiv a license to display the preprint in perpetuity. It is made available under aCC-BY-NC-ND 4.0 International license.

M. Zielinski, M. Steinegger, M. Pacholska, T. Berghammer, S. Bodenstein, D. Silver, O. Vinyals, A. W. Senior, K. Kavukcuoglu, P. Kohli and D. Hassabis (2021). "Highly accurate protein structure prediction with AlphaFold." Nature **596**(7873): 583-589.
Katsinelos, T., M. Zeitler, E. Dimou, A. Karakatsani, H. M. Muller, E. Nachman, J. P. Steringer, C. Ruiz de Almodovar, W. Nickel and T. R. Jahn (2018). "Unconventional Secretion Mediates the Trans-cellular Spreading of Tau." Cell Rep **23**(7): 2039-2055.
Kellner, R., E. Vollmeister, M. Feldbrugge and D. Begerow (2011). "Interspecific sex in grass smuts and the genetic diversity of their pheromone-receptor system." PLoS Genet **7**(12): e1002436.
Kikhney, A. G., C. R. Borges, D. S. Molodenskiy, C. M. Jeffries and D. I. Svergun (2020). "SASBDB: Towards an automatically curated and validated repository for biological scattering data." Protein Sci **29**(1): 66-75.
Koepke, J., F. Kaffarnik, C. Haag, K. Zarnack, N. M. Luscombe, J. Konig, J. Ule, R. Kellner, D. Begerow and M. Feldbrugge (2011). "The RNA-binding protein Rrm4 is essential for efficient secretion of endochitinase Cts1." Mol Cell Proteomics **10**(12): M111 011213.
Konarev, P. V., V. V. Volkov, A. V. Sokolova, M. H. J. Koch and D. I. Svergun (2003). "PRIMUS: a Windows PC-based system for small-angle scattering data analysis." Journal of Applied Crystallography **36**: 1277-1282.
Langner, T. and V. Gohre (2016). "Fungal chitinases: function, regulation, and potential roles in plant/pathogen interactions." Curr Genet **62**(2): 243-254.
Langner, T., M. Ozturk, S. Hartmann, S. Cord-Landwehr, B. Moerschbacher, J. D. Walton and V. Gohre (2015). "Chitinases Are Essential for Cell Separation in Ustilago maydis." Eukaryot Cell **14**(9): 846-857.
Lee, M. C., E. A. Miller, J. Goldberg, L. Orci and R. Schekman (2004). "Bi-directional protein transport between the ER and Golgi." Annu Rev Cell Dev Biol **20**: 87-123.
Li, G. Z., J. P. Vissers, J. C. Silva, D. Golick, M. V. Gorenstein and S. J. Geromanos (2009). "Database searching and accounting of multiplexed precursor and product ion spectra from the data independent analysis of simple and complex peptide mixtures." Proteomics **9**(6): 1696-1719.
Manalastas-Cantos, K., P. V. Konarev, N. R. Hajizadeh, A. G. Kikhney, M. V. Petoukhov, D. S. Molodenskiy, A. Panjkovich, H. D. T. Mertens, A. Gruzinov, C. Borges, C. M. Jeffries, D. I. Svergun and D. Franke (2021). "ATSAS 3.0: expanded functionality and new tools for small-angle scattering data analysis." Journal of Applied Crystallography **54**(1).
Marmeisse, R., A. Guidot, G. Gay, R. Lambilliotte, H. Sentenac, J. P. Combier, D. Melayah, L. Fraissinet-Tachet and J. C. Debaud (2004). "Hebeloma cylindrosporum- a model species to study ectomycorrhizal symbiosis from gene to ecosystem." New Phytol **163**(3): 481-498.
Masson, G. R., J. E. Burke, N. G. Ahn, G. S. Anand, C. Borchers, S. Brier, G. M. Bou-Assaf, J. R. Engen, S. W. Englander, J. Faber, R. Garlish, P. R. Griffin, M. L. Gross, M. Guttman, Y. Hamuro, A. J. R. Heck, D. Houde, R. E. Iacob, T. J. D. Jorgensen, I. A. Kaltashov, J. P. Klinman, L. Konermann, P. Man, L. Mayne, B. D. Pascal, D. Reichmann, M. Skehel, J. Snijder, T. S. Strutzenberg, E. S. Underbakke, C. Wagner, T. E. Wales, B. T. Walters, D. D. Weis, D. J. Wilson, P. L. Wintrode, Z. Zhang, J. Zheng, D. C. Schriemer and K. D. Rand (2019). "Recommendations for performing, interpreting and reporting hydrogen deuterium exchange mass spectrometry (HDX-MS) experiments." Nat Methods **16**(7): 595-602.
Mirdita, M., K. Schutze, Y. Moriwaki, L. Heo, S. Ovchinnikov and M. Steinegger (2022). "ColabFold: making protein folding accessible to all." Nat Methods **19**(6): 679-682.
Nickel, W. and C. Rabouille (2018). "Unconventional protein secretion: Diversity and consensus." Semin Cell Dev Biol **83**: 1-2.
Petoukhov, M. V., D. Franke, A. V. Shkumatov, G. Tria, A. G. Kikhney, M. Gajda, C. Gorba, H. D. T. Mertens, P. V. Konarev and D. I. Svergun (2012). "New developments in the ATSAS program package for small-angle scattering data analysis." Journal of Applied Crystallography **45**: 342-350.
Philipp, M., K. P. Hussnaetter, M. Reindl, K. Muntjes, M. Feldbrugge and K. Schipper (2021). "A Novel Potent Carrier for Unconventional Protein Export in Ustilago maydis." Front Cell Dev Biol **9**: 816335.

bioRxiv preprint doi: https://doi.org/10.1101/2024.02.29.582524; this version posted March 2, 2024. The copyright holder for this preprint (which was not certified by peer review) is the author/funder, who has granted bioRxiv a license to display the preprint in perpetuity. It is made available under aCC-BY-NC-ND 4.0 International license.

Poloni, A. and J. Schirawski (2016). "Host specificity in Sporisorium reilianum is determined by distinct mechanisms in maize and sorghum." Mol Plant Pathol **17**(5): 741-754.
Rabouille, C. (2017). "Pathways of Unconventional Protein Secretion." Trends Cell Biol **27**(3): 230-240.
Rabouille, C., V. Malhotra and W. Nickel (2012). "Diversity in unconventional protein secretion." J Cell Sci **125**(Pt 22): 5251-5255.
Rapoport, T. A. (2007). "Protein translocation across the eukaryotic endoplasmic reticulum and bacterial plasma membranes." Nature **450**(7170): 663-669.
Reindl, M., S. Hansch, S. Weidtkamp-Peters and K. Schipper (2019). "A Potential Lock-Type Mechanism for Unconventional Secretion in Fungi." Int J Mol Sci **20**(3).
Reindl, M., J. Stock, K. P. Hussnaetter, A. Genc, A. Brachmann and K. Schipper (2020). "A Novel Factor Essential for Unconventional Secretion of Chitinase Cts1." Front Microbiol **11**: 1529.
Schekman, R. (2010). "Charting the secretory pathway in a simple eukaryote." Mol Biol Cell **21**(22): 3781-3784.
Sparn, C., A. Meyer, R. Saleppico and W. Nickel (2022). "Unconventional secretion mediated by direct protein self-translocation across the plasma membranes of mammalian cells." Trends Biochem Sci **47**(8): 699-709.
Stahelin, R. V., J. L. Scott and C. T. Frick (2014). "Cellular and molecular interactions of phosphoinositides and peripheral proteins." Chem Phys Lipids **182**: 3-18.
Steringer, J. P. and W. Nickel (2018). "A direct gateway into the extracellular space: Unconventional secretion of FGF2 through self-sustained plasma membrane pores." Semin Cell Dev Biol **83**: 3-7.
Stock, J., P. Sarkari, S. Kreibich, T. Brefort, M. Feldbrugge and K. Schipper (2012). "Applying unconventional secretion of the endochitinase Cts1 to export heterologous proteins in Ustilago maydis." J Biotechnol **161**(2): 80-91.
Svergun, D. I. (1992). "Determination of the Regularization Parameter in Indirect-Transform Methods Using Perceptual Criteria." Journal of Applied Crystallography **25**: 495-503.
Temmerman, K., A. D. Ebert, H. M. Muller, I. Sinning, I. Tews and W. Nickel (2008). "A direct role for phosphatidylinositol-4,5-bisphosphate in unconventional secretion of fibroblast growth factor 2." Traffic **9**(7): 1204-1217.
Terfruchte, M., B. Joehnk, R. Fajardo-Somera, G. H. Braus, M. Riquelme, K. Schipper and M. Feldbrugge (2014). "Establishing a versatile Golden Gate cloning system for genetic engineering in fungi." Fungal Genet Biol **62**: 1-10.
Viotti, C. (2016). "ER to Golgi-Dependent Protein Secretion: The Conventional Pathway." Methods Mol Biol **1459**: 3-29.
Wales, T. E., K. E. Fadgen, G. C. Gerhardt and J. R. Engen (2008). "High-speed and high-resolution UPLC separation at zero degrees Celsius." Anal Chem **80**(17): 6815-6820.
Walter, P. and G. Blobel (1980). "Purification of a membrane-associated protein complex required for protein translocation across the endoplasmic reticulum." Proc Natl Acad Sci U S A **77**(12): 7112-7116.
Wedlich-Soldner, R., M. Bolker, R. Kahmann and G. Steinberg (2000). "A putative endosomal t-SNARE links exo- and endocytosis in the phytopathogenic fungus Ustilago maydis." EMBO J **19**(9): 1974-1986.
Weinberger, A., F. C. Tsai, G. H. Koenderink, T. F. Schmidt, R. Itri, W. Meier, T. Schmatko, A. Schroder and C. Marques (2013). "Gel-assisted formation of giant unilamellar vesicles." Biophys J **105**(1): 154-164.
Weinzierl, G., L. Leveleki, A. Hassel, G. Kost, G. Wanner and M. Bolker (2002). "Regulation of cell separation in the dimorphic fungus Ustilago maydis." Mol Microbiol **45**(1): 219-231.
Zehe, C., A. Engling, S. Wegehingel, T. Schafer and W. Nickel (2006). "Cell-surface heparan sulfate proteoglycans are essential components of the unconventional export machinery of FGF-2." Proc Natl Acad Sci U S A **103**(42): 15479-15484.
Zeitler, M., J. P. Steringer, H. M. Muller, M. P. Mayer and W. Nickel (2015). "HIV-Tat Protein Forms Phosphoinositide-dependent Membrane Pores Implicated in Unconventional Protein Secretion." J Biol Chem **290**(36): 21976-21984.

bioRxiv preprint doi: https://doi.org/10.1101/2024.02.29.582524; this version posted March 2, 2024. The copyright holder for this preprint (which was not certified by peer review) is the author/funder, who has granted bioRxiv a license to display the preprint in perpetuity. It is made available under aCC-BY-NC-ND 4.0 International license.

Zhou, L., T. Obhof, K. Schneider, M. Feldbrugge, G. U. Nienhaus and J. Kamper (2018). "Cytoplasmic Transport Machinery of the SPF27 Homologue Num1 in Ustilago maydis." Sci Rep **8**(1): 3611.

Zweng, S., G. Mendoza-Rojas and F. Altegoer (2023). "Simplifying recombinant protein production: Combining Golden Gate cloning with a standardized protein purification scheme." arXiv.